UiT
THE ARCTIC
UNIVERSITY
OF NORWAY

Faculty of Science and Technology
Department of Physics and Technology

A compact portable resonance probe system for *in situ* measurements of snow conditions.

—

Jakop Reistad

FYS-3921 Master's thesis in Electrical Engineering
January 2018

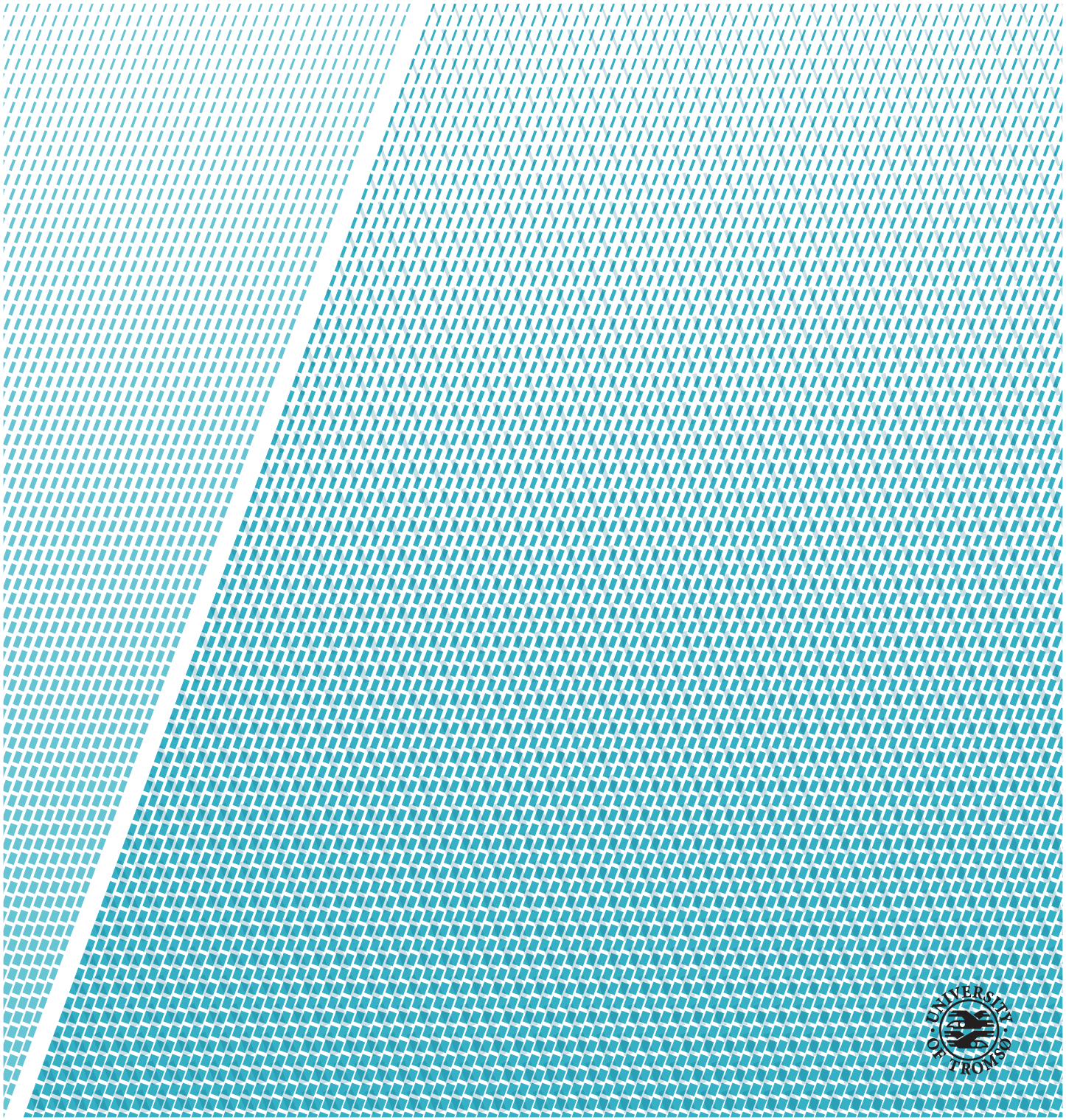

Abstract

A resonance probe for measuring the dielectric properties of snow in terms of the resonance frequency is described and tested. The dielectric properties of snow are closely related to the density and the water content in snow. Having a probe capable of measuring the dielectric properties is therefore a useful tool for anyone working with quantitative descriptions of snow properties. *In situ* measurements with the snow sensor system have been conducted during the autumn semester of 2017. To verify and correlate the *in situ* measurements, numerical simulations and density measurements have also been conducted. Measurements performed *in situ* have been compared to analytical data and numerically simulated data. By comparing the results, relative errors ranging from 1.5 to 7.2% were found between the measured resonance frequency, and the numerically simulated resonance frequency.

Acknowledgements

First and foremost, I would like to thank my supervisor, professor Svein Ketil Jacobsen. His enthusiasm and optimism in the period of writing this thesis have been very motivating.
I would also like to thank my office mates, John Hallvard and Luis for being good friends, and for keeping a positive atmosphere at the office.
Last but not least, I would like to thank Marte for keeping me alive, and being supportive and patient during my last two years of studying.

Jakop Reistad
Tromsø, January 2018

Contents

Abstract **i**

Acknowledgements **iii**

List of Figures **ix**

List of Tables **xi**

1 Introduction **1**
1.1 Motivation 1
1.2 Aim of thesis 2
1.3 Related work 3
1.4 Structure of Thesis 4

I Theory **5**

2 Microwave Theory **7**
2.1 TEM waves 8
2.2 Dielectric constant 9
2.3 Dielectric loss effects 9
2.4 Microstrip transmission line 10
2.5 Microwave Vector Network analyzer (VNA) 12

3 Microstrip Resonance probe **15**
3.1 General resonance theory 15
3.2 Resonance frequency of covered microstrip line 17
3.3 Fano Resonance 18
3.3.1 Fano resonance in snow 20

4 Snow theory **23**
4.1 Mixing theory 24
4.2 Snow Morphology 26
4.3 Snow density and Liquid Water Content 27

II System description **31**

5 Probe design and features **33**
5.1 Electrical design 33
5.2 Mechanical design 34
5.3 Mini Radio Solutions' MiniVNA tiny 36
5.4 Case study: Vector network analyzer comparison 38

6 Numerical simulations **41**
6.1 CST Microwave studio 41
6.1.1 Numerical simulation output data 43

7 *In situ* measurement techniques **45**
7.1 Snow probe measurements 45
7.2 Density measurements 46
7.3 Liquid Water measurements 47

III Results **51**

8 Quasi analytical approximations of the resonance frequency **53**
8.1 Solving for air medium 53
8.2 Solving for snow superstrate resonance frequency 54

9 Numerical simulations **55**
9.1 Numerical simulations of the sensor in air 55
9.2 Numerical simulations for snow media 57

10 *In situ* measurements **59**
10.1 *In situ* measurements 1/11 60
10.2 *In situ* measurements 6/12 62

11 Comparing results **67**
11.1 Correlation between analytical model, simulations and *in situ measurements* 67

IV Conclusion & Discussion **71**

12 Discussions **73**

13 Conclusions **75**
13.1 Future work 75

Bibliography **77**

List of Figures

2.1 The electromagnetic spectrum 7
2.2 Microstrip transmission line 10
2.3 S-parameters 12
2.4 Vector network analyzer block diagram 13

3.1 Resonance curve example 16
3.2 Multi layer microstrip 18
3.3 Coupled fano resonance model 19
3.4 Fano and Lorentzian resonance profiles 20

4.1 Snowflakes size vs. temperature 24
4.2 Relative permittivity of water 25
4.3 Relative permittivity of snow versus liquid content 26
4.4 Snow morphology diagram 27
4.5 Snow water content, density and dielectric constant 28
4.6 Snow density plotted vs. dielectric constant 29

5.1 Microstrip probe dimensions 34
5.2 Snow probe photograph 35
5.3 MRS MiniVNA tiny 37
5.4 VNA Blue screenshot 37
5.5 Fieldfox N9916A 38
5.6 Comparison between MiniVNA and fieldfox 40

6.1 Snow probe in CST MWS 41
6.2 Gaussian pulse in time domain 43
6.3 Simulation data example 44

7.1 Examples of density cutters 46
7.2 Image of density cutters used in this thesis 47

8.1 Resonance frequency solved quasi analytical 54

9.1 Numerical simulation plot 56

9.2 Resonance frequency determined by numerical simulation . 57
9.3 Amplitude and bandwidth vs. snow depth 58

10.1 Photograph of snowpack 06/12 59
10.2 Measured resonance frequency in the snowpack 61
10.3 Density at depth of measurement 63
10.4 Measured resonance frequency in the snowpack 64
10.5 Amplitude and bandwidth vs. snow depth 65

11.1 Correlation between analytical, numerical and *in situ* result . 68
11.2 Correlation between analytical, numerical and *in situ* result . 69

List of Tables

5.1 MiniVNA Specifications 36
5.2 Agilent Fieldfox N9916A Specifications 39

7.1 Description of hand test for liquid water content in snow . . 48

10.1 Snow density, measured 1/11/2017 60
10.2 Snow density, measured 6/12/2017 62

11.1 Relative errors between measured resonance frequency and reference data 68
11.2 Relative errors in the measured normalized resonance frequencies. 70

1 Introduction

1.1 Motivation

Monitoring of the snowpack is important for several fields of research and engineering. Major areas of application include (but not limited to) geophysics/geology, meteorology and climate research, civil security and hydro electric power prediction.
We live in a time where research on climate and global rising temperatures has never been more important. Several scientific fields of research are trying to understand the connection between declining snow reservoirs and global temperature of the earth [51], [6]. The extent of snow coverage play an important part in the way our climate system works. It is therefore necessary to monitor this parameter with high resolution both temporally and spatially. This is only achievable using remote sensing techniques [13].
With seasonal changes, the accumulated snow during the cold winter season will act as a reservoir of water during the warmer season [37], [63]. This is one of our must important resources, both as hydrodynamic energy [48] and water itself being essential for all forms of life. In addition to being a resource, it can also pose a significant treat to civil security. Rapid snow melting regularly cause mass floods and unstable ground conditions and thereby landslides etc. It is therefore very important be able to monitor the volume of snow, as well as wetness and density.
Snow in its original form also pose a treat to population living in avalanche exposed areas. In December 2015 [23] a large avalanche claimed two lives and injured many, as well as causing mass destruction in Longyearbyen, Svalbard.

Better monitoring of avalanche risk, and improved forecasting could greatly improve safety for those living in exposed areas. By forecasting avalanche risk, and triggering an avalanche under controlled conditions, the amount of destruction and cost to society could be reduced. In many areas avalanche risk assessments are carried out by routinely performing *in situ* measurements. Many places will likely continue to do it this way, as it is easy to get started with. Just walk outside and record a measurement. If a capable, easy to use instrument is made available, a lot of information about the condition of the snowpack can be collected. After all, satellite monitoring is very expensive, and requires very advanced processing.
That being said, a lot of research is done [62], [18], and is ongoing by using Synthetic Aperture Radar (SAR) for monitoring avalanche risk. However, progress in the field of remote sensing will not be possible without a lot of experimental field work. All remote sensing techniques relying on variation in permittivity, with radar being the most important, requires *in situ* measurements for verifying and correction of data [14]. Therefore improvements in performance and user-friendliness of *in situ* instruments will also be beneficial for further developments of remote sensing techniques.
In situ snow instruments are commercially available on the market today, but these systems are based on old hardware, and are relatively bulky compared to typical modern electronics. By utilizing computationally powerful modern integrated circuits, there is a potential to develop a versatile, small and relatively inexpensive system. Possible improvements in accuracy and resolution should also be investigated.

1.2 Aim of thesis

The aim of this thesis is to describe and test a new sensor for determining the dielectric constant of snow. Its characteristics will be investigated by using both analytical models and numerical simulation software. Real world *in situ* measurements should be performed, on snow in different locations and of varying quality (density, wetness). *In situ* density samples should be collected for use as reference data. In the end, all available data must be analysed. Analytical, numerical and experimental data should be compared and checked for agreement against existing literature.

The sensor system consists of two microstrip resonators and data acquisition hardware. The working principle is that the resonance behaviour is dependent on the loading material. Numerical simulations of the sensor system will be used to generate reference data. This gives the opportunity to simulate snow like

conditions, without varying external factors. The effect of snow parameters can be studied isolated of each other, and isolated from the background disturbance. By using modern simulation software, adequate numerical resolution and accurate models, the simulation results should show a near ideal response of the sensor system.
There are existing work available in the literature on the topic of quasi-analytical models for microstrip resonators. This will be applied on the resonators used in this thesis, to give some theoretical baseline numbers on resonance frequencies.
Experimental data must be collected by performing *in situ* measurements with the snow sensor in the field. This should be done during varying condition of the snow pack. When field measurments are collected with the resonant sensor, accompanying density measurement should be done also.
In the end, all gathered data will be combined in an attempt to establish a semi empirical relation between sensor output and the dielectric constant. This will include comparing analytical, numerical and experimental data in addition to data available in the literature. The ultimate goal is to determine the usefulness of this sensor design, and to investigate how well it can measure the dielectric constant of snow, and in turn calculate density and possibly wetness.

1.3 Related work

Scientific studies of snow and snow properties *per se* have been conducted for centuries [38]. However, techniques and equipment to perform quick and easy quantitative measurements of snow parameters are limited to recent decades. Even though some equipment are available today, methods such as digging snow profiles and the hand test [55] are widely used. Both rely heavily on experience and subjective opinion of the operator.

During the 1950's and 1960's a number of studies on the dielectric properties of snow were published ([12], [31], [15]). The correlation between physical snow and dielectric properties were theorized, and experiments were conducted.

Progress in electronic technology during the 1970s and '80s made snow sensor systems possible. Multiple such systems, relying on dielectric principles, were developed. A flat plate condenser, used to characterise the dielectric response in the snow were developed by Ambach and Denoth [1].

Tiuri et al., at the Helsinki Radio Laboratory developed the *Snow Fork* in 1984 [58] and [46]. This is a complete measurement system for determining the

complex dielectric constant in the snow pack, as well as wetness and density. It consist of the probe itself, as well as an analog computer to calculate the results.
In 1994 Kendra and Ulaby developed their snow probe [28], which is similar in design and function to the Snow Fork developed by Tiuri et al., 1984.
Since then, no new developments have been published on portable *in situ* instruments for performing snow measurements.

1.4 Structure of Thesis

Part I contains necessary background theory which the techniques used and described in this paper build upon. This includes general microwave theory, theory on microwave transmission lines and resonators, theory on the interaction between microwaves and dielectric mediums (focusing on snow). Snow theory, with focus on dielectric properties is presented.

Part II is a description of the sensor system. All the individual parts are described and their use in this thesis is explained. This includes equipment used, as well as software and procedures.

Part III of this thesis contains the results. This part is subdivided into quasi analytical approximations, numerical simulations, and real world *in situ* measurements. The results are presented, and compared to each other.

In **part IV** conclusions are drawn, and the results are discussed. Possible future work needed to the system are suggested and discussed.

Part I

Theory

2

Microwave Theory

Radio frequency (RF) spans from 100 MHz to 3 Ghz while microwaves typically is referred to as signals from 3 GHz to 300 Ghz [43]. This corresponds to an electrical wavelength ranging from 3 metres to 1 millimetre. The spectrum is divided into the following sub-bands:

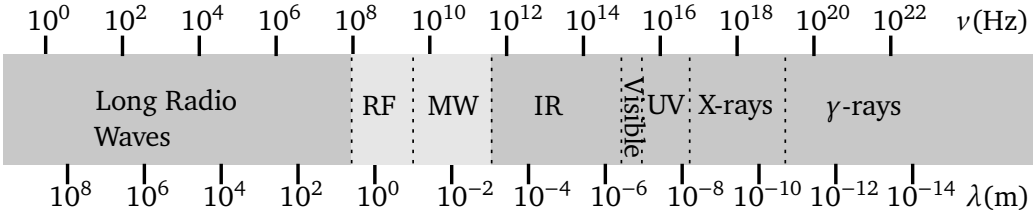

Figure 2.1: The electromagnetic spectrum

The theory presented in this thesis all builds upon the theory of electromagnetic waves (EM waves), and how they propagate in different media. Although EM waves have the ability to propagate without the presence of medium, i.e. in free space, it is the properties of the medium that determines the behaviour of propagation.
The behaviour of EM waves can be completely described in both time and space by Maxwells equations. They are expressed in an integral form or in a differential form. Below Maxwells four equations are written out in their integral form [20]:

$$\text{Gauss' Law: } \oiint_{\partial\Omega} = \mathbf{E} \cdot d\mathbf{S} = \frac{1}{\epsilon_0} \iiint_{\Omega} \rho \, dV \tag{2.1}$$

$$\text{Gauss' magnetism law: } \oiint_{\partial\Omega} = \mathbf{B} \cdot d\mathbf{S} = 0 \tag{2.2}$$

$$\text{Maxwell-faraday equation: } \oint_{\partial\Sigma} \mathbf{E} \cdot d\ell = -\frac{d}{dt} \iint_{\Sigma} \mathbf{B} \cdot d\mathbf{S} \tag{2.3}$$

$$\text{Amperes law: } \oint_{\partial\Sigma} \mathbf{B} \cdot d\ell = \mu_0 \iint_{\Sigma} \mathbf{J} \cdot d\mathbf{S} + \mu_0 \epsilon_0 \frac{d}{dt} \iint_{\Sigma} \mathbf{E} \cdot d\mathbf{S} \tag{2.4}$$

Gauss' law states that the electric field leaving a volume is proportional to the charge inside. Gauss magnetism law gives that there are no magnetic monopoles, and the total magnetic flux piercing a closed surface is zero. The meaning of Maxwell-Faradays law is that voltage accumulated in a closed circuit is proportional to the change in magnetic flux inside it. Amperes law states that electric current and changes in electric fields are proportional to the magnetic field circulating the area they pierce [20].

By using these four equations, all aspects of EM waves propagating in space and time can be described in terms of the electric field (**E**-field), the magnetic field (**H**-field) and the fundamental constants of electric permittivity and magnetic permeability. This is known as field theory, and is the core of classical theoretical electromagnetics.

2.1 TEM waves

Microwaves can propagate with or without the presence of a medium. In order to use microwaves to carry information within some sort of device, or from one such device to another, we use transmission lines or waveguides. The signal energy is carried by an electromagnetic field. If the transmission line is pointing in the z direction, the **E**-field and **H**-field can be decomposed into transverse (x, y direction) and axial (z direction) components. If the **E**-field have no axial component ($\mathbf{E}_z = 0$), the wave is called transverse electric (TE). If the **H**-field have no axial component ($\mathbf{H}_z = 0$), the wave is known a transverse magnetic (TM). If the wave have both $\mathbf{E}_z = 0$ and $\mathbf{H}_z = 0$, the wave is known as Transverse Electromagnetic (TEM) [9]. Transmission lines such as coaxial cables and stripline can fully support propagation of TEM waves [43].

2.2 Dielectric constant

As stated above, the behaviour of propagation is determined by the medium, and the propagation velocity is given by the relation $1/\sqrt{\mu\epsilon}$. In vacuum, the relation $c_0 = 1/\sqrt{\mu_0\epsilon_0}$ is true, where $\mu_0 \approx 1.26 \times 10^{-6}$ [1] is the permeability of free space, and $\epsilon_0 \approx 8.85 \times 10^{-12}$ [2] is the permittivity of free space. This gives the speed of light in a vacuum $c_0 = 299\ 792\ 458$ m/s.
For media on earth, μ and especially ϵ will be be different to that of free space. However, for most naturally occurring materials, including snow, $\mu \simeq \mu_0$ [52].
The permittivity of a given medium is typically given in relation to the permittivity of free space. This is referred to as the relative permittivity, or the *dielectric constant*, often denoted ϵ_r. The dielectric constant of dry air at sea level is 1.000569 [25], but 1.0 is typically used for simplifying calculations. In short terms, it means that air and vacuum behaves identically with respect to being a dielectric.
The dielectric constant describes how (much) a material influences an electric field applied to it. Electric fields (and magnetic fields) interact with materials in two ways; storing energy and dissipating energy. Energy storage describes the lossless portion of energy exchange between the field and the material, while energy dissipation occurs when energy is absorbed by the material, and dissipated as heat. The dielectric constant is therefore expressed as a complex quantity. The storage of energy is represented by the real part, while the dissipation or loss of energy is the imaginary part. [9]:

$$\epsilon_r(\omega) = \epsilon_r'(\omega) - j\epsilon_r''(\omega) \tag{2.5}$$

where $\epsilon_r'(\omega)$ is the real part, and $j\epsilon_r''(\omega)$ is the imaginary part of the complex dielectric constant. A third useful material parameter is the *loss tangent* $\tan\delta$. It is given as the ratio between the imaginary and and the real part of the dielectric constant [9]:

$$\tan\delta = \frac{\epsilon_r''}{\epsilon_r'} \ . \tag{2.6}$$

The loss tangent describes the relation between energy dissipated by the electric field versus the energy stored by the electric field, in the material.

2.3 Dielectric loss effects

When an electromagnetic wave propagates trough a medium it carries a certain amount of energy. As stated above, the imaginary part of the dielectric constant

1. $\mu_0 = 1.25663706 \times 10^{-6}\ m\ kg\ s^{-2}\ A^{-2}$
2. $\epsilon_0 = 8.85418782 \times 10^{-12}\ m^{-3}\ kg^{-1}\ s^4\ A^2$

$j\epsilon_r''(\omega)$, dictates the loss in a dielectric medium. For a wave travelling in a lossless medium, such as a vacuum, no losses occur. But all real life dielectric media have a finite, non zero loss. Propagation loss in lossy media occurs in to different forms; *absorption loss* and *scattering loss*. Absorption loss is due to the finite ϵ_r'' in the medium, similar to conduction loss in a wire [43]. The energy lost due to absorption is dissipated as heat in the medium. Scattering occurs in heterogeneous or rough media, or on the boundaries between homogeneous media. As a propagating wave encounter changing intrinsic impedance, reflections will occur, and some amount of the wave energy will be scattered.

2.4 Microstrip transmission line

The Microstrip transmission line is one of the most popular types of planar transmission lines, primarily because it is easy to manufacture, and well suited for use on a printed circuit board with integrated circuits[43]. A thin conductor (typically copper) of width W is laminated or etched on top of a grounded substrate with thickness d:

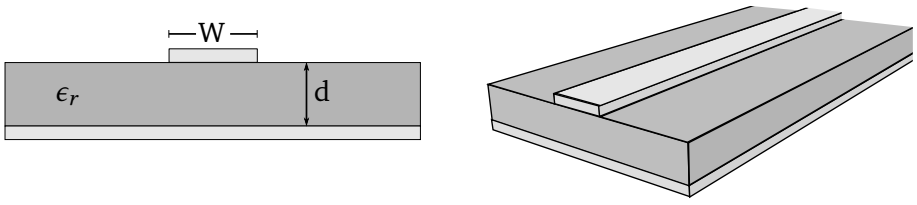

(a) Side view of a Microstrip transmission line

(b) 3D sketch of a microstrip transmission line

Figure 2.2: Microstrip transmission line

If the dielectric substrate is removed, it becomes a simple two-wire transmission line with a flat conductor over a ground plane in a homogeneous medium, e.g. air ($\epsilon_r = 1$). This would make it a simple TEM wave transmission line. However, the presence of the dielectric, particularly the fact that the dielectric does not fill the region above the conductor, complicates the behaviour and analysis of the microstrip line [43]. If the dielectric on all sides of the strip was one homogeneous dielectric ϵ_r, the phase velocity v_p would be $c/\sqrt{\epsilon_r}$. But because there are different dielectric constants in the surrounding medium

and the substrate, the phase velocity is different as well. This means that a microstrip line can not support pure TEM waves [43]. However, in most practical applications, we have a very thin substrate ($d \ll \lambda$), and the fields are considered quasi-TEM [43]. Then the phase velocity and the propagation constant can be expressed as

$$v_p = \frac{c}{\sqrt{\epsilon_e}} \tag{2.7}$$

$$\beta = k_0\sqrt{\epsilon_e} \tag{2.8}$$

where ϵ_e is the effective dielectric constant, and k_0 is the free space wave number. Because some of the field lines are in the medium outside (air), and some are in the substrate, the effective dielectric satisfies the relation

$$1 < \epsilon_e < \epsilon_r \tag{2.9}$$

which means that the effective dielectric constant lies in between that of the substrate, and that of air. An approximation of the effective dielectric constant for a microstrip line is given by [43]

$$\epsilon_e = \frac{\epsilon_r + 1}{2} + \frac{\epsilon_r - 1}{2}\frac{1}{\sqrt{1 + 12d/W}}\,. \tag{2.10}$$

In order to design a useful microstrip line, we want to minimize the reflection when feeding power into it. The refection coefficient is given as [43]

$$\Gamma = \frac{Z_1 - Z_0}{Z_1 + Z_0} \tag{2.11}$$

where Z_1 is the characteristic impedance of the microstrip being fed power, and Z_0 is the characteristic impedance of the feeding line. As we can see, $Z_1 = Z_0$ makes the reflection coefficient equal to zero, and no power is reflected.
Most scientific equipment uses transmission lines with a characteristic impedance of 50Ω. In order to design a 50Ω we use this approximation [43]

$$Z_0 = \begin{cases} \frac{60}{\sqrt{\epsilon_e}} \ln\left(\frac{8d}{W} + \frac{W}{4d}\right) & \text{for } W/d \leq 1 \\ \frac{120\pi}{\sqrt{\epsilon_e}\left[W/d + 1.393 + 0.667\ln\left(W/d + 1.444\right)\right]} & \text{for } W/d \geq 1 \end{cases} \tag{2.12}$$

We can calculate the W/d ratio for a given characteristic impedance Z_0, and substrate dielectric constant ϵ_r by [43]

$$\frac{W}{d} = \begin{cases} \frac{8e^A}{e^{2A} - 2} & \text{for } W/d < 2 \\ \frac{2}{\pi}\left[B - 1 - \ln\left(2B - 1\right) + \frac{\epsilon_r - 1}{2\epsilon_r}\left\{\ln\left(B - 1\right) + 0.39 - \frac{0.61}{\epsilon_r}\right\}\right] & \text{for } W/d > 2 \end{cases} \tag{2.13}$$

where

$$A = \frac{Z_0}{60}\sqrt{\frac{\epsilon_r + 1}{2}} + \frac{\epsilon_r - 1}{\epsilon_r + 1}\left(0.23 + \frac{0.11}{\epsilon_r}\right) \tag{2.14}$$

$$B = \frac{377\pi}{2Z_0\sqrt{\epsilon_r}} \tag{2.15}$$

2.5 Microwave Vector Network analyzer (VNA)

A *Vector Network analyzer* is a tool for characterizing RF and Microwave devices in terms of transmission and reflection parameters over a given frequency range. Examples of such devices are filters, antennas, couplers, cables, amplifiers, attenuators or resonators. When a device is tested with a VNA, it is characterized by its Scattering Parameters, also known a S-parameters. A N-port device, has N^2 S-parameters. A typical two port device therefore has four separate S-parameters; S11, S21, S12 and S22. These are typically presented in an S-matrix:

$$[S] = \begin{bmatrix} S11 & S12 \\ S21 & S22 \end{bmatrix}. \tag{2.16}$$

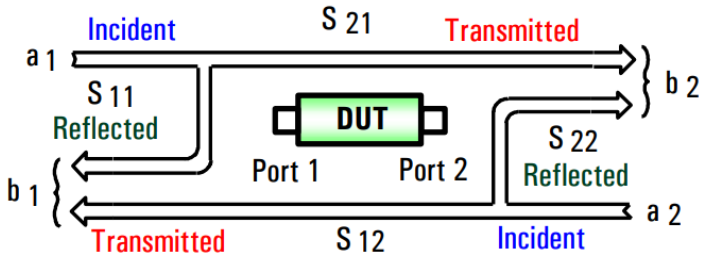

Figure 2.3: Graphical diagram showing S-parameters. Reprinted from [57].

S-parameters give a relative power measurement, plotted against the frequency. S11 is the ratio of reflected power to the incident power. S21 is transmitted power in relation to incident power. S12 the amount of power reflected back trough to the source port, while S22 is the power reflected from the device under test (DUT) back to the receiver port. Having an impedance matched termination to the device under test is very important. If the terminations are

not perfectly matched this will cause additional reflections, which is not caused by the DUT. This will reduce the accuracy of the measured S-parameters [57]. Expressing the S-parameters in common measurement terms, S11 is a measurement of the reflection coefficient (input matching), S21 is the forward transmission coefficient (gain/loss), S22 is the reverse reflection coefficient (output matching) and S12 is the reverse transmission coefficient or the isolation.

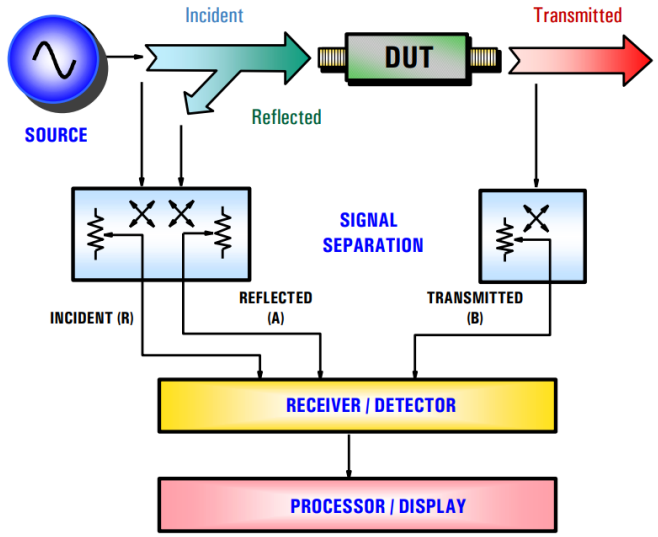

Figure 2.4: Generalized Block diagram of a Vector Network Analyzer. Reprinted from [57].

Figure 2.4 shows a block diagram representation of a general VNA. The components in a VNA can be divided into four layers; signal source, signal separation, receiver and display and processing unit. The signal source consist of a sweeping frequency generator. Its job is to output a frequency range which is used to excite the Device Under Test. The performance of this unit depends on a frequency reference which is used to synthesize the frequency range. The stability of the reference frequency dictates the accuracy of the output frequency. The next stage is the signal separation block. It performs two main tasks. Firstly it takes a small portion of the incident signal as a reference for ratioing later. This is typically done with a directional coupler. This is a multi port device which passes most of the signal energy straight trough with low loss, but separates out a small portion of the signal energy for later reference. The second part of the signal separation block is to separate the incident and the reflected signal power. This can be done with either a directional coupler or a directional bridge.
The receiver block is fed by three separate signals, incident, reflected and

transmitted. The signals are downconverted by a mixer and sampled by an analog-to-digital (ADC) converter. The sampling frequency of the ADC must obviously meet the requirements of the Nyquist sampling theorem [35]. Having a higher sampling rate allows oversampling which improves the dynamic range by sampling more signal power, and reducing noise by averaging. The use of oversampling will however reduce the bandwidth resolution, so it is a trade off [57].

Vector Network Analyzers are complex instruments which contain many different parts. Traditionally, VNAs have been manufactured by large companies developing their own parts, specially designed for use in Network Analyzers. High development costs, as well as the use of proprietary parts make these VNAs extremely expensive, especially for extended frequency ranges.
Advances in cell phone and computer technology have made high frequency technology such as wireless networking very popular. As devices get smaller and smaller, integrated circuits become increasingly capable and powerful. It is possible to get off-the-shelf hardware which are rated up to a few GHz. With the use modern circuit board design techniques, and readily available components, a range of compact, cheap VNAs have emerged [3] [4] [5]. Performance wise, these units can not be compared to industrial standard instruments, but they offer decent performance at lower frequencies, at a much lower price. Open source software can often add special functionality to these units.

3. http://pocketvna.com/
4. https://www.sdr-kits.net/index.php?route=web/pages&page_id=11_11
5. http://miniradiosolutions.com/54-2/

3

Microstrip Resonance probe

3.1 General resonance theory

An oscillating system (whether mechanical, electromagnetic, acoustic etc.) tends to oscillate at its natural frequency. The natural frequency is an inherent physical property of the system. If the system is excited with an external force with a frequency content containing the natural frequency, the system will start to oscillate. When external force contain a large amount of energy at the natural frequency, the system will resonate at higher amplitude [19].
The two main parameters governing a resonant system are the resonant frequency f_0 and the *quality factor* (Q-factor).

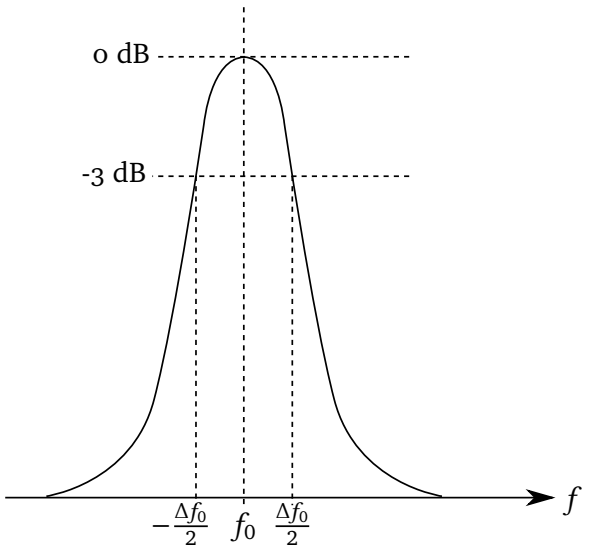

Figure 3.1: A general (symmetric) resonance curve

The resonant frequency, as described above, is the natural frequency of a system. If a system is exited with a frequency similar of equal to its resonance frequency, it will *resonate*, i.e. oscillate with a higher amplitude. Each system could have multiple resonance frequencies. The Q-factor is a measure of loss in a resonator, or the ability a resonator has to store energy. A high quality factor indicates low loss, i.e. a given energy input to the system will last a large number of oscillations. The Q-factor is defined as [43]

$$Q = 2\pi f \, \frac{\text{average energy stored}}{\text{average loss/second}} \, . \tag{3.1}$$

Then there is the loaded quality factor, given by the relation [7]

$$Q_L = \frac{f_0}{\Delta f} \tag{3.2}$$

where f_0 is the resonance frequency and Δf is the -3dB bandwidth.
This also applies to electromagnetic systems, where the energy is carried by electromagnetic waves.
In this thesis we will study microstrip resonators. One can construct a half-wavelength microstrip resonator from a piece of open circuited microstrip. Its length is given by: [43]

$$\ell = \frac{\lambda}{2} = \frac{v_p}{2f} = \frac{c}{2f\sqrt{\epsilon_e}} \;\Rightarrow\; f = \frac{c}{2\ell\sqrt{\epsilon_e}} \tag{3.3}$$

where ℓ is the length of the microstrip line, f is the resonant frequency, λ is the wavelength, c is the speed of light and ϵ_e is the effective dielectric constant

of the microstrip line. When the microstrip line resonator is in air, the resonant frequency will be dependent of the effective dielectric constant (ϵ_e), which is constrained by $1 < \epsilon_e < \epsilon_r$ where ϵ_r is the dielectric constant of the substrate. When the microstrip line is covered by a dielectric layer (e.g. snow) the resonance frequency, characteristic impedance, phase velocity and Q-factor of the line change because of changes in the dielectric properties, loss tangent and thickness of the covering layer [4]. This means that the medium surrounding the microstrip line resonator is directly related to the resonance frequency, and the Q-factor.
As we see in equation (3.3), f_0 have a proportionality to $1/\sqrt{\epsilon}$. This means that if ϵ increase, we expect the resonance frequency to decrease, and vice versa. This principle can be utilized to measure ϵ, if one can establish an empirical relation between change in resonance frequency to the change in ϵ.

3.2 Resonance frequency of covered microstrip line

A dielectric cover affects the resonance frequency and effective dielectric constant, as have been studied in the literature [29]. Shavit [45] used Spectral domain analysis to study resonance and input impedance. Verma et al. [59] used the variational technique with transmission line model to calculate resonance frequency. Bahl et al. [5] used Fourier domain variational technique to calculate effective permittivity and Pozar [42] studied resonance using method of moments. However, all these techniques are complex and time consuming, and not suitable for direct integration in CAD software. Kumar and Malathi [29] presents an extended closed form design equation for calculating the resonance frequency of multilayer rectangular microstrip. They show good agreement between theory and experimental results. The approximation is given as [29]:

$$f_r = \frac{c}{2\left(L + 2\Delta L\right)\left(\epsilon_{eff}(f)\right)^{1/2}} \tag{3.4}$$

where c is the the velocity of light in free space, L is the length of the rectangular patch, ΔL is the length of the extension due to end effect and $\epsilon_{eff}(f)$ is the frequency dependent effective dielectric constant of the multilayer structure. ϵ_{eff} is approximated by (derived in detail in [65]):

$$\epsilon_{eff}(f) = \epsilon_r' - \frac{\epsilon_r' - \epsilon_e}{1 + P(f)} \tag{3.5}$$

where ϵ_r' is the equivalent permittivity of a single substrate microstrip line, and ϵ_e is the effective permittivity of a single substrate microstrip line, which relates to ϵ_r' by the approximation given in equation (2.10) also used in section 2.4:

$$\epsilon_e = \frac{\epsilon_r + 1}{2} + \frac{\epsilon_r - 1}{2} \frac{1}{\sqrt{1 + 12d/W}} \,. \tag{3.6}$$

This quasi analytic approximation given in (3.4), can be solved to calculate the resonance frequency of a rectangular microstrip line with substrates and superstrate. By following detailed derivation in [65], we can input our physical dimensions, including line length L and line width W. We also input superstrate height h_3, and superstrate dielectric constant ϵ_{r3} as show below in figure 3.2. The thickness of the substrate between the copper strip and the groundplane has a height h_2 and dielectric constant ϵ_{r2}. It is also possible to solve for an additional substrate, shown in figure 3.2 as the bottom layer, with height h_1 and dielectric constant ϵ_{r1}.

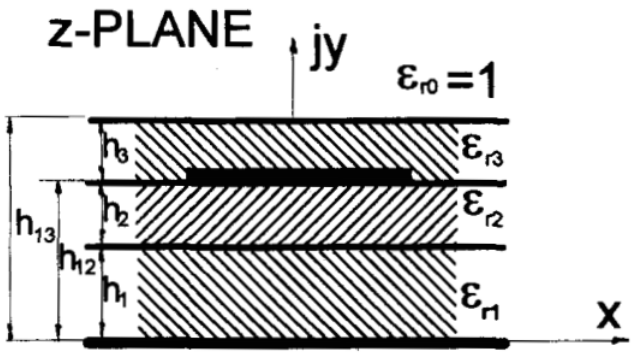

Figure 3.2: Rectangular microstrip with multiple sub- and superstrates, and an equivalent single substrate line. Reprinted from [65].

3.3 Fano Resonance

Resonance phenomena occur everywhere, and always show a frequency dependence. However, the resonance curve rarely look as uniform and symmetric around the center frequency as the one shown in figure 3.1. Instead, the resonance line shape usually has some degree of asymmetry. Ugo Fano [16] established a theoretical understanding on the subject of asymmetric resonance curves. Fano experimentally confirmed (trough his work in atomic and molecular physics) that that the asymmetric profile could be attributed to coupling between resonant effects. The experiments carried out by Fano analyses the

resonant peaks in the spectrum generated by ionizing various molecular configurations of helium gas. The asymmetry was found to be caused by resonant coupling between a discrete excited state and a continuum of states not excited by the ionization process. An analogy to this coupling effect is shown below in figure 3.3.

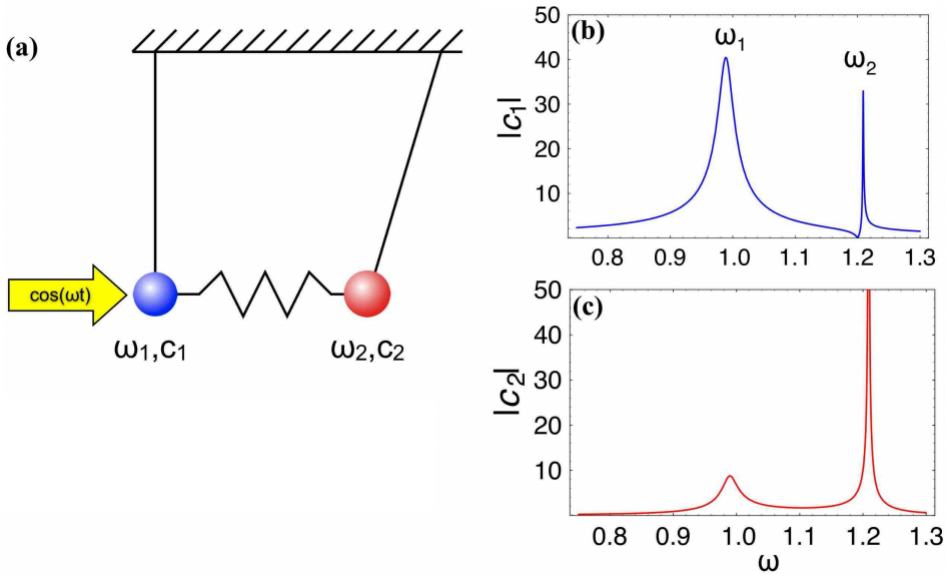

Figure 3.3: Coupling between resonant processes generating asymmetric fano profile. Reprinted from [36].

The figure above shows two dampened harmonic oscillators, with respective resonant frequencies ω_1 and ω_2. The left (blue) oscillator is excited by an external force, and there is a coupling to the one on the right (red), visualized as a spring. As the exciting force is acting on the blue resonator, energy is coupled between the two resonators. Plot (b) show the resulting resonance spectrum for the blue resonator, while plot (c) show the resonance of the red resonator. As we can see in plot (b), the driven oscillator clearly show an asymmetric peak at ω_2. This peak is caused by resonant coupled back from the non-driven oscillator [36].
The general expression for an asymmetric Fano resonance curve is given by [26]:

$$T(f) = \frac{1}{1+q^2}\frac{(\epsilon+q)^2}{1+\epsilon^2}, \text{ where } \epsilon = \frac{(f-f_r)}{\Gamma}. \tag{3.7}$$

The lower case q parameter is the coupling parameter, responsible for the amount of asymmetry in the curve. ϵ is the reduced energy, and f_r and Γ is the peak frequency and the bandwidth, respectively. By taking the limit of equation

(3.3), we get the formula of a classic, symmetric Lorentzian resonance curve:

$$\lim_{q\to\infty} \frac{1}{1+q^2}\frac{\left(\epsilon+q^2\right)}{1+\epsilon^2} = \frac{1}{1+\epsilon^2} \tag{3.8}$$

Below is a plot of the fano profile with various q-values, as well as the classical Lorentzian resonance curve.

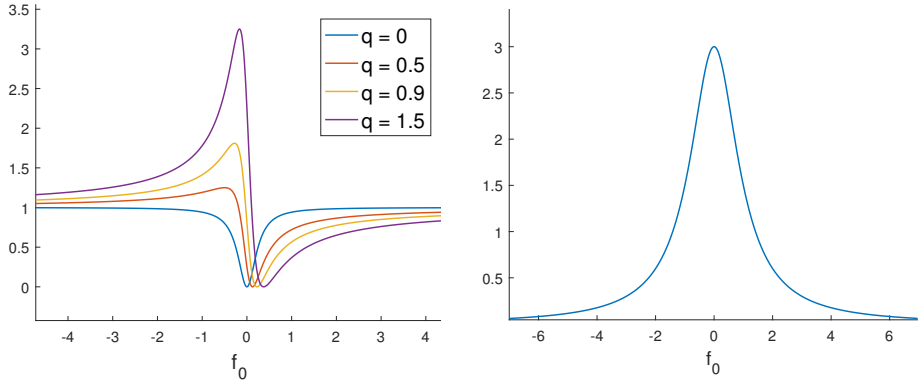

(a) Asymmetric fano curves

(b) Symmetric Lorentzian curve

Figure 3.4: Microstrip transmission line

With q=0 we observe an anti-resonant dip at the resonant frequency. With values $0 < q < \infty$, the profile will be a skewed resonance. For $q \to \infty$ we get a Lorentzian resonance curve.

3.3.1 Fano resonance in snow

We observe asymmetric resonance curves in the spectrum generated by the snow sensor described in this thesis. The theoretical connection between the shape of the resonance curve, and the dielectric properties of the snow being measured, could be caused by coupling between resonant effects in snow. However, not on an atomic or molecular level, as described by Fano. Instead the resonant coupling could be dependant on snow crystal structure, or snow particle size and distribution. As the snow sensor uses frequencies in the low gigahertz range, the wavelength is in the order of several centimetres. This is in the same order of magnitude as the size of particles and crystals in snow. When the wavelength is in the same range as physical dimensions in a resonating setup, the resonance properties will be affected.
If the incoming RF wave energy (from the snow probe) excites a particular resonant mode given by structures in the snowpack, the asymmetry could be

caused by mutual coupling to not directly excited resonant structures. However, the subject of asymmetric resonance curves in snow as a dielectric medium, has seen little research. This must be investigated further in order to understand the physics causing the asymmetry.

4

Snow theory

By the most simple description, snow is a mixture of air, ice and (potentially) liquid water. Ice is obviously water in its frozen state, and when it is frozen at regular atmospheric conditions it has a density of 0.917 g/cm^3 [3]. This type of ice is known as normal hexagonal crystalline ice (Ice I_h). It is one of 17 known crystalline phases of water, however mainly Ice I_h appears naturally on earth. The study of ice crystalline phases is a whole field of research on its own [33]. Snow flakes are a special type of precipitation where ice crystals are allowed to grow because of specific atmospheric conditions. When specific temperature, water vapour supersaturation and water vapour pressure occurs in precipitating clouds, ice crystals grow and form snow flakes [32] [34] [24]. The size of the forming crystals depends on temperature, as can be seen in figure (4.1). Large snowflakes, above two centimetres in size, will only occur in a small temperature range from about 0° C to -4° C.

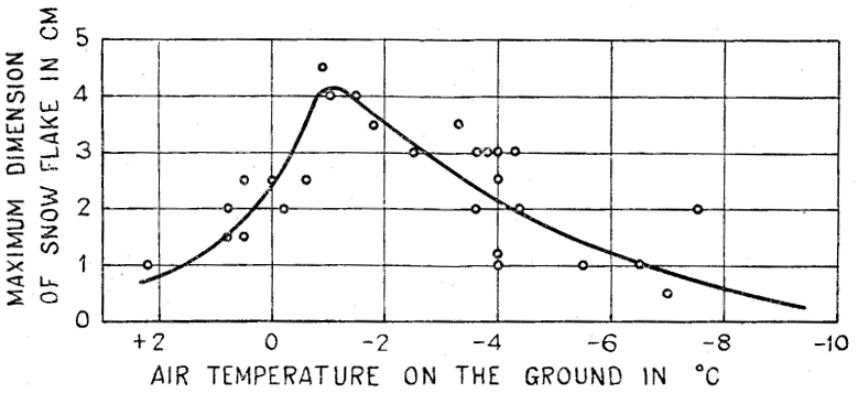

Figure 4.1: Snow flake size in relation to temperature. Reprinted from [34].

The relation between snow with different air-ice-water composition and ice crystal structure and their respective dielectric properties have been widely studied in the literature. Air and dry snow (consisting mostly of air) have similar, low permittivity values. The dielectric constant of dry snow therefore lies within a small range. Water on the other hand, has a much higher relative permittivity. Therefore the dielectric constant of wet snow vary a lot more, depending on liquid water content [10].

4.1 Mixing theory

As snow consists of multiple materials, with different dielectric properties, it is considered as a heterogeneous dielectric. The theoretical study of dielectric media with a mixed composition is known as mixing theory. A large number of studies present theoretical and empirical derived expressions for understanding the effective dielectric properties of a mixed material. Polder and van Santeen [41] published the first mixing theory model, and it has since been referred to as *Polder and van Santeen mixing theory*. It shows that the effective permittivity of mixed material does not only depend on the composition of the parts, but also the distribution and structure. The dependence on the shape of the individual particles is also investigated. Analytical models for mixtures containing ellipsoidal, spherical, disc shaped and needle shaped particles were presented. As snow crystals take on many different shapes, these models have been been applied to snow by Sihvola and Kong [47].
As mentioned above, dry snow has a relatively low variability when it comes to permittivity, as it consists mostly of air. The density dependence of ϵ'_d of dry snow is practically linear below $\rho_d = 0.5 g/cm^3$ [21].

Snow containing liquid water behaves radically different as a dielectric. The permittivity of water is a complex quantity, and is both frequency and temperature dependent [2]. As can be read from figure (4.2), water has a permittivity of about 90 at low temperature and relatively low frequency. Therefore, even a small inclusion of liquid water makes a big impact on the dielectric constant of snow.

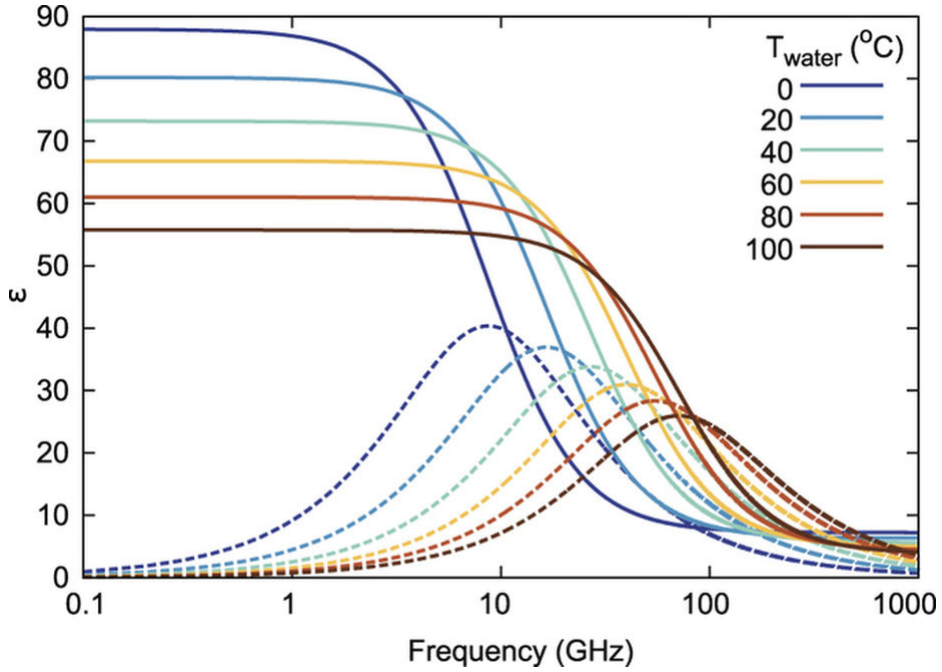

Figure 4.2: Complex relative permittivity of water as a function of frequency and in relation to temperature. Reprinted from [2]

Colbeck [10] divides wet snow into two distinct regimes, called *pendular* and *funicular*. The pendular regime is for snow of low wetness, where air is continuous throughout and water is contained in isolated inclusions. The fenicular regime occurs in snow of high wetness, where water is continuous throughout the snow volume, with isolated air bubbles.

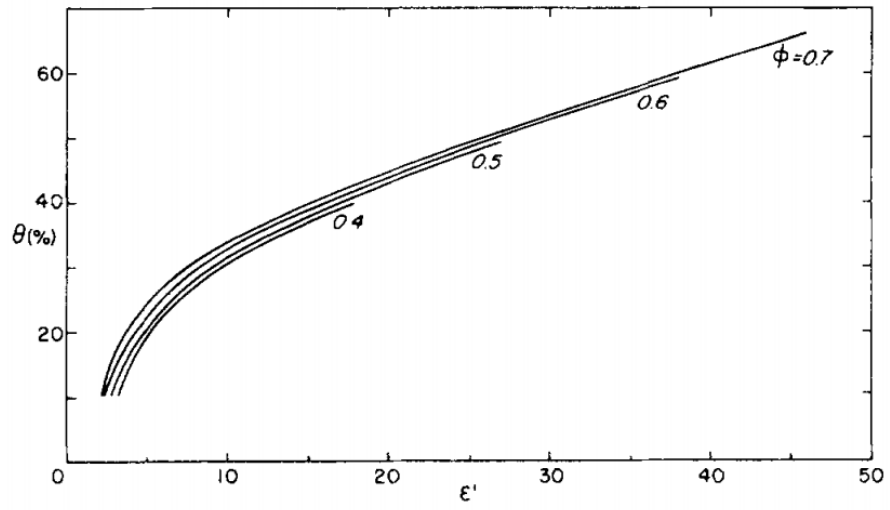

Figure 4.3: Dielectric constant of wet snow versus liquid water content for different values of porocity (ϕ). Reprinted from [10]

The above figure describe the relation between water content in snow in the fenicular regime. It can be seen that for water content higher than 30 percent the permittivity is linearly dependent of the water content. Each of the separate lines represents different porosities in the snowpack, but as shown in the plot (figure 4.3) they follow similar profiles.

4.2 Snow Morphology

As mentioned above, snow crystal growth occurs in atmospheric clouds with the correct temperature, pressure and water vapour supersaturation. In figure (4.4), a graphical representation of crystal growth, in relation to vapour supersaturation and temperature is shown.

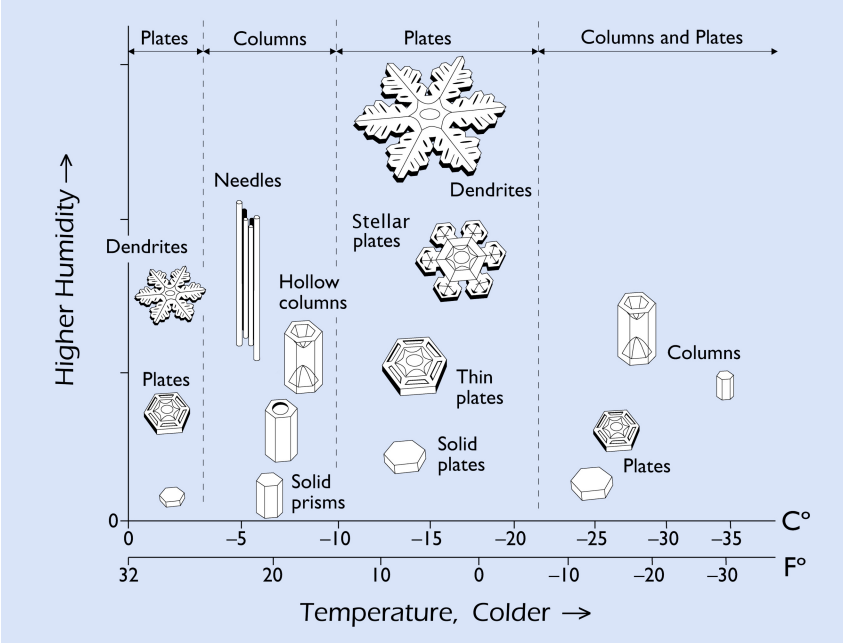

Figure 4.4: Snow morphology diagram. Reprinted from Snow Crystals web page [1]

We observe that larger and more complex crystalline shapes require higher humidity in the air to be able to grow. Surdyk and Fujita [53] found that the real part of the dielectric constant mainly depends on the density. The complex part however, i.e. the loss part of the dielectric constant is dependent on both frequency and particle size. At lower frequency the main loss effect are wave energy being absorbed and dissipated as heat in the medium. When the frequency increases, or particle size increases (particle size gets comparable to wavelength) scattering becomes the dominating loss effect [22].

4.3 Snow density and Liquid Water Content

The complex dielectric constant in the medium is the most important property of the snowpack in relation to an instrument using microwave frequencies. However, for most researchers or engineers, *in situ* probing is just a tool used to determine snow density or water content, or both. The working principles of the instrument is less important than ease of use and accuracy. It is therefore very important to understand the connection between dielectric properties and physical properties, primarily density and wetness. Tiuri and Sihvola [46] have

1. Snow Crystals web page `http://www.snowcrystals.com/morphology/morphology.html`

published both theoretical and experimental work on this area, and presents a nomogram (figure 4.5) where wetness and density can be read from the real and imaginary part of the dielectric constant.

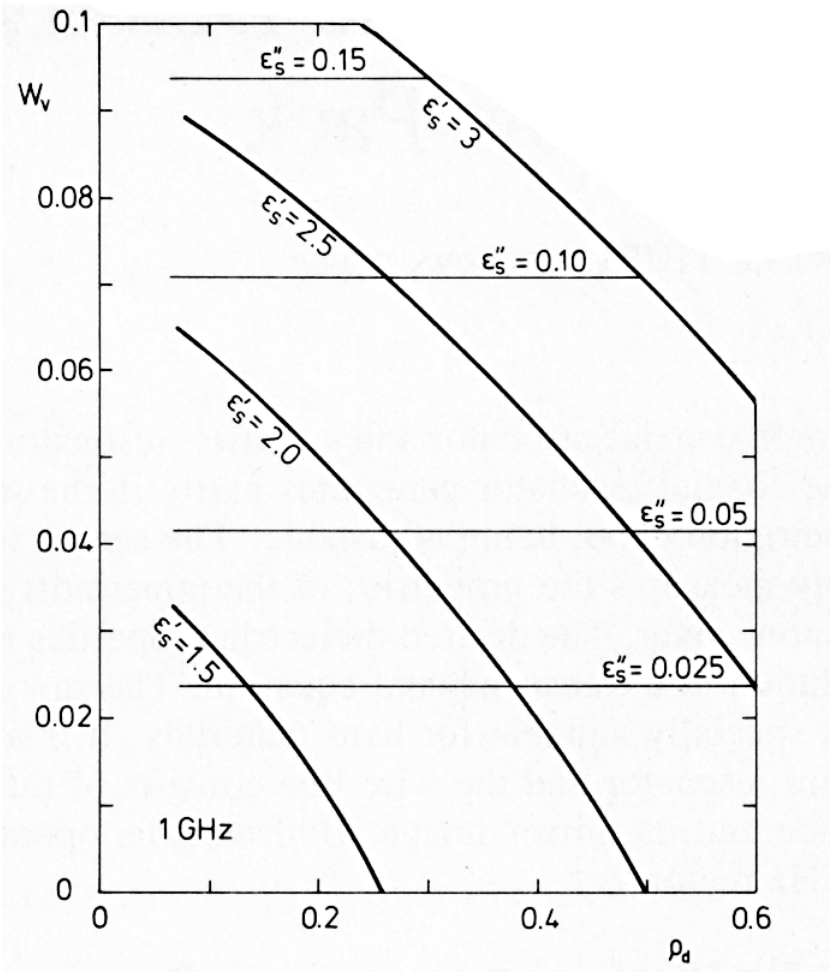

Figure 4.5: The relation between snow water content, snow density and the complex dielectric constant. Evaluated at 1 GHz. Reprinted from [46]

Tiuri have also conducted a lot of in situ measurements to determine the relationship between the density of snow, and the real part of the dielectric constant. In figure 4.6, the Tiuri et al. [58] published the results of many *in situ* measurements in dry snow.

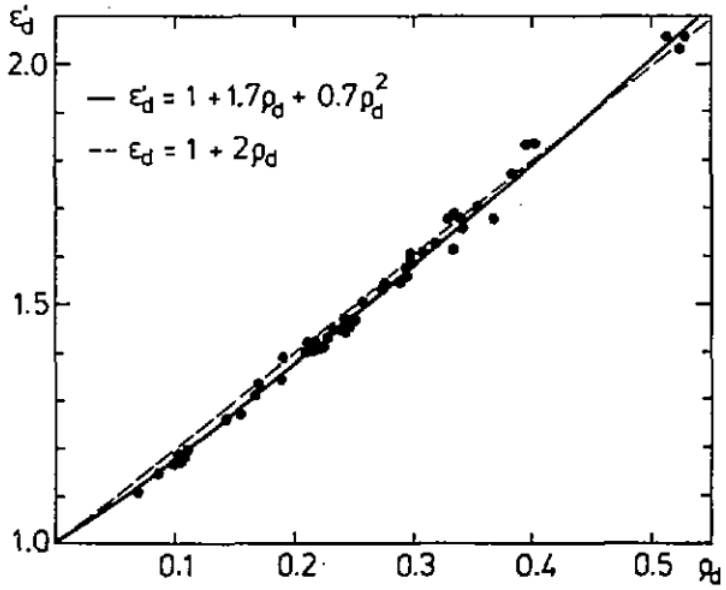

Figure 4.6: Empirical relation between snow density and the real part of the dielectric costant. Reprinted from [58]

The results from figure 4.6 was the basis for an empirical model for the relation between the density of dry snow, and the real part of the dielectric constant. It is given in [58]:

$$\epsilon_r' = 1 + 1.7\rho_d + 0.7\rho_d^2 \tag{4.1}$$

where ϵ_r' is the real part of the dielectric constant, and ρ_d is the density of dry snow.

Part II

System description

5

Probe design and features

The probe presented in this thesis consists of three main components:

- Sensor head designed by Prof. Svein Ketil Jacobsen.
- Commercially available USB-based Vector Network Analyzer.
- Java based software, running on host computer.

5.1 Electrical design

The main part of the sensor consist of two flat prongs, held together by a 3D-printed housing. The two prongs are identical, each with an open ended microstrip transmission line facing each other. Signal energy is coupled into the input side microstrip trough a capacitive gap (i.e. a physical gap in the microstrip). See dimensional drawing in figure 5.1 below.

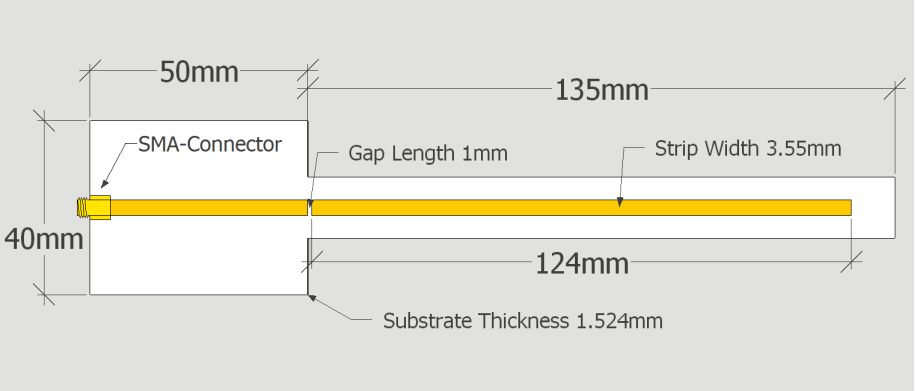

Figure 5.1: 2D top down dimensional drawing of the microstrip prongs.

The microstrip prongs are a made using Rogers RO4003C substrate. It is a woven glass fibre and ceramic laminate, made to have better dimensional tolerances than regular printed circuit board material. Detailed specifications are are available in the RO4000 series datasheet by Rogers [11]. The substrate has a dielectric constant ϵ_r of 3.38 ±0.05 and a dielectric loss tangent, δ, of 0.0021 at 2.5 GHz. Copper thickness on both sides of the board is 35 μm, and the entirety of the back side is covered by a copper ground plane.

5.2 Mechanical design

Mechanically, the sensor is made up of two pieces of the microstrip board shown in the last section. They are mounted in a 3D printed enclosure, with the top side of each microstrip facing each other (see figure 5.2). The enclosure serves several purposes, it provides the structure needed to mount the resonant microstrip prongs at a fixed distance. Secondly, the body itself functions as an area to hold the device when performing measurements. The back part of the case also contains the Vector Network Analyzer used to excite the prongs, and measure the response.

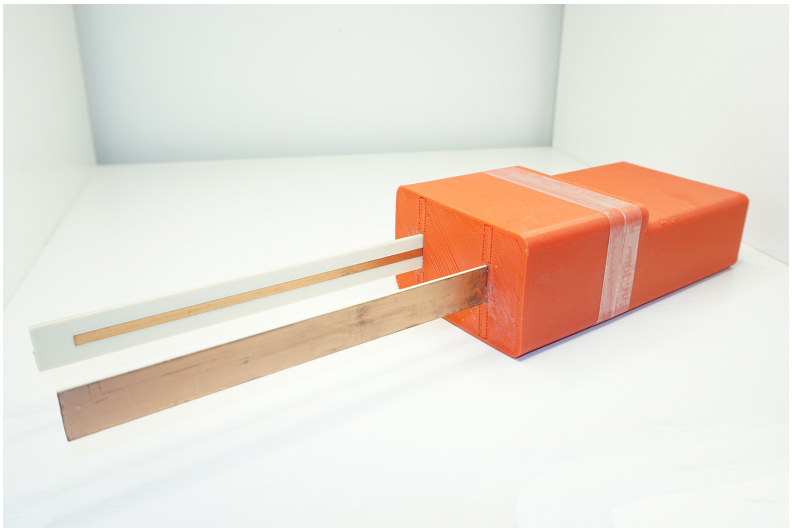

Figure 5.2: Photograph of the final snow sensor system

The housing is printed using Acrylonitrile Butadiene Styrene (ABS) filament. It is a common thermoplastic, widely used for injection moulding, but also popular for 3D-printing. The printed case has good mechanical properties, such as impact resistance and toughness, which is very useful when handling the sensor in the field. The printed walls are waterproof, and the plastic does not absorb moisture. By using an appropriate sealant in the in the joints and openings in the body, it could potentially by made water tight.
As a dielectric material, ABS has a dielectric constant of $\epsilon_r \approx 2.57$, and a dielectric loss tangent $\delta = 0.00469$ [8]. The overall length of the instrument is 28 cm, and the weight is 195g (including MiniVNA Network Analyzer).

Some concerns have been raised about the rigidity of the prongs, in regards to usage in hard snow. This is important, as deflection or deformations of the prongs would probably influence the accuracy of the measurements. For future use in hard snow, the prongs could be stiffened by gluing a lengthwise running, perpendicular, piece along the back of each prong. This would result in a structure resembling a T-shaped beam, which would be more resistant to twisting and deflection.

5.3 Mini Radio Solutions' MiniVNA tiny

In addition to the microstrip prongs themselves, the instrument uses a small Vector Network analyzer (VNA) to generate an output signal, and capture the transmitted signal. This small unit, made by Mini Radio Solutions[1], measures approximately 6×6 cm^2, and provides a measurement bandwidth of 1 MHz to 3 GHz. Detailed specifications are given below in table 5.1.

Table 5.1: MiniVNA tiny specifications. Obtained from [49].

MiniVNA Tiny	
Specification	Value
Frequency range	1 MHz to 3 GHz
No of Ports	Two. Can measure S11 and S21
RF output power	-6dBm @ 500 MHz
Power consumption	370mA 5 V over USB
Connectors	SMA connectors
Dynamic range	up to 70 dB 500 MHz
Boot loader for firmware upgrades	Yes
Software availability	Windows, Linux, Mac
Android Mobile Phone software	Yes
Data export formats	jpg, excel, zplot, s2p, pdf

The Network Analyzer is USB-based, meaning that the hardware itself does little more than generating an output signal, and capturing the transmitted signal. All processing, display and storage of data is done in software on the host computer. The software used in this thesis is developed by third party user Dietmar Krause [2], and is built in the Java programming language. It features both a graphical user interface, allowing functionality similar to a desk top network analyzer, and a command line interface. As it is running in Java, it can be used on very many platforms, as java is widely supported. The command line interface could be utilized in a future version of the snow sensor to perform automated scan and data storage.

1. Mini Radio Solutions: `http://miniradiosolutions.com/`
2. Software available at `http://vnaj.dl2sba.com/`.

Figure 5.3: Image of the MiniVNA tiny, reprinted from Mini Radio Solutions web page.[3]

In addition to the java application, there also exist a mobile phone application for smartphones running android operating system, known as Blue VNA. This enables you to perform measurements with a very lightweight and compact setup. The probe connects to a smartphone using USB On-the-go functionality. This enables the USB-port in the phone to function as a USB host, just like a computer. It is supported by most newer phones running android.

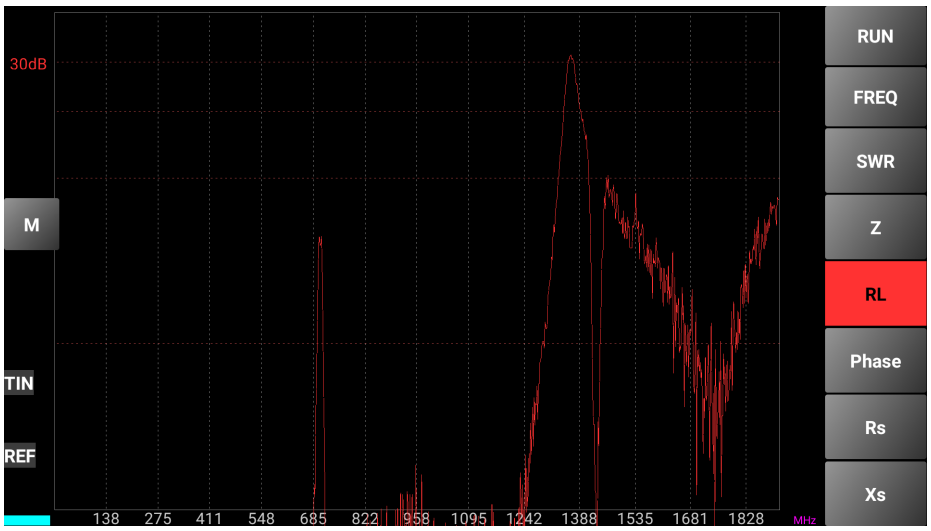

Figure 5.4: Android app VNA blue screenshot

3. MRS web page: `http://miniradiosolutions.com/54-2/`

In order to perform a measurement you connect the instrument to your phone with a USB cable, and open the app. The you select the wanted frequency range, and click RUN. The app then starts performing the scan, the acquisition time is a couple of seconds. Then the results are shown on the screen.
In figure 5.4 above, a screenshot of a snow scan performed in the app is shown. The vertical axis in the app can not be zoomed, so it is difficult to visualize the full dynamic range of the measurements. However, when the data is exported to a .csv file for processing, they are complete.

5.4 Case study: Vector network analyzer comparison

As known from the previous section, we use a MRS MiniVNA tiny in this thesis. This is a compact and inexpensive Vector Network Analyzer, available for about $550 [4]. This is a lot cheaper than a typical bench top industrial VNA. In the scope of this thesis however, a full size VNA would not be possible to integrate into the sensor system, and having to carry a large additional instrument would defeat the purpose of the sensor described in this thesis.

Figure 5.5: Photograph of the Fieldfox N9916A, reprinted from Keysight web page.[5]

4. https://www.hamradio.com/detail.cfm?pid=H0-013596
5. Keysight web page: https://www.keysight.com/en/pdx-x201925-pn-N9916A/fieldfox-handheld-microwave-analyzer-14-ghz?&cc=NO&lc=eng

In this section we will compare the performance of the miniVNA tiny, to an Agilent Fieldfox N9916A (shown above in figure 5.5). This unit is sold as a combination analyzer, as it has capabilities both as a spectrum analyzer, and as a vector network analyzer. It is a portable device, and it has a rubber like protective housing, making it suited for field use. In terms of size, this unit measures about 30×20 cm^2, and weighs 3 kg, and is therefore much smaller than a typical benchtop VNA. It is however, much larger than the MiniVNA. The current typical retail price of the Keysight Fieldfox N9916A is $16370, which is about 30 times the price of the MiniVNA. The specifications of the Fieldfox N9916A is given in table 5.2 below.
If we compare the size of the MiniVNA network analyzer to the size of a state of the art bench top network analyzer, the differences are even clearer. Keysight PNA-L series[6] VNAs measure 50×28×48 cm^3, and have a weight of 25 kg.

Table 5.2: Agilent Fieldfox N9916A Specifications. Obtained from [56].

Agilent Fieldfox N9916A	
Specification	Value
Frequency range	30 kHz to 14 GHz
No of ports	Two. Measures all four S.parameters
RF output power	-4 dBm
Dynamic Range	91 dB
Trace Noise	0.004 dBrms
Overall amplitude accuracy	±0.5 dB
Battery	Rechargeable Li-Ion
Weight	3 kg

In terms of specifications given by the manufacturers, there are a number of differences. The much more expensive Agilent model has a much larger frequency range, a higher power output and much more dynamic range. It is capable of measuring all four S-parameters in a single setup, while the MiniVNA is only capable of measuring S11 and S21, without flipping the device around.
It is no surprise that the specifications of the 30 times more expensive unit exceeds the cheaper unit. However, we want to investigate how different they perform when used as intended in this thesis, measuring the snow sensor response. This is tested by measuring the transmission response of the snow probe in air with both the Agilent instrument, and the MiniVNA. The results are plotted below in figure 5.6.

6. Keysight PNA vector analyzers: `https://www.keysight.com/en/pcx-x205186/pna-network-analyzers-300-khz-to-11-thz?cc=US&lc=eng`

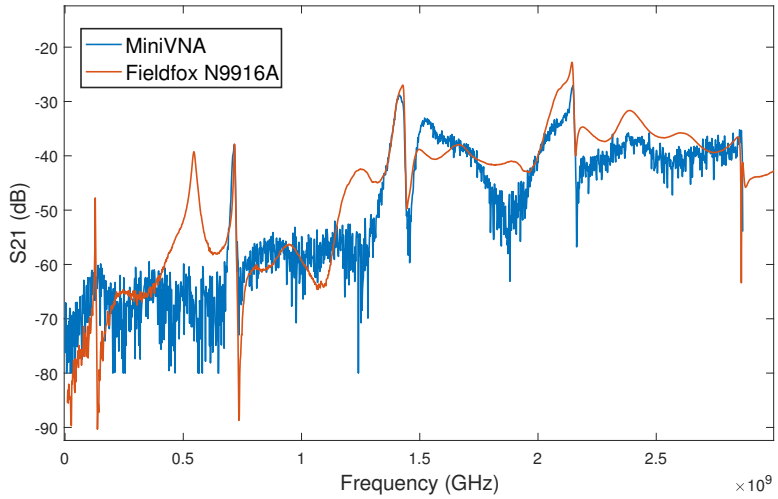

Figure 5.6: Comparison of S21 plot from MiniVNA and Agilent Fieldfox N9916A.

The overall response measured by the two instruments are similar, and most importantly, the resonance peaks line up. However, the curve produced by the Fieldfox is a lot smoother than the one from the MiniVNA. This is especially visible in low areas of the plot (i.e. non resonant parts). There could be a number of reasons for this, but most likely this is a result of better receiver and sampling hardware in the Fieldfox unit. With a much larger enclosure, there is more room to ensure good overall noise performance, by incorporating shielding of important components.
The most important take away from this comparison, is that the resonance peaks seem to coincide very well. Especially along the frequency axis, which is most important parameter for measurements in dry snow, they line up well. The most important peak, namely the second one (around 1.4 GHz), show center frequency and bandwidth discrepancies of less than 2 MHz. For the peak amplitude there is a discrepancy between the two of 2.1 dB.
Another strange discrepancy is the peak located at about 550 MHz in the Fieldfox plot. This peak is not present in the MiniVNA plot. This is probably caused by a physical dimension in the measurement setup becoming comparable to the given wavelength. At 550 MHz, the wavelength is about 54 centimeters. In order to connect the Fieldfox VNA to the probe, the 3D-printed back cover had to be removed. As the back of the unit was open, some object in the room at the correct distance can be the culprit of this resonance peak. However, this was not further investigated.

6

Numerical simulations

6.1 CST Microwave studio

Numerical simulations are performed by using CST Microwave Studios, developed by Dassault Systemes. It is widely used in the industry, to design, analyze and optimize microwave components before production [60].
A dimensionally accurate, three dimensional CAD model is drawn to represent the sensor system (shown in figure 6.1 below).

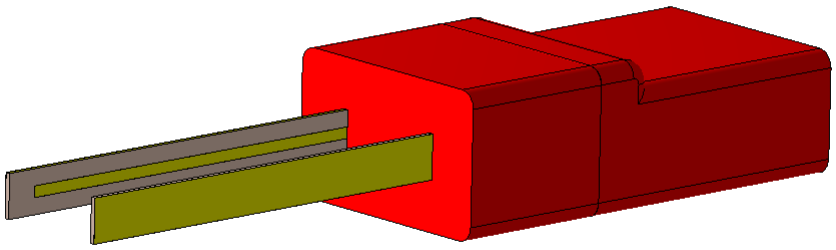

Figure 6.1: A screenshot of the snow probe model used in the CST software.

The software contains a number of different numerical solvers [1], and can analyse our model in both the time and the frequency domain. In this thesis, all simulations are done with the time domain solver. A detailed description on how to use this solver, as well as a description on how it works is given in [54].
The time domain solver in CST MWS uses the numerical technique known as Finite Integration Technique. It is based on a discretized version of Maxwell's equations in their integral form. Before the numerical simulations can be run on our model, some preparations are needed. We need to set up waveguide ports, which is where simulated signal energy is injected into our numerical model. In the actual snow probe system, this would be done trough SMA connectors. When setting up the waveguide ports for a microstrip line, a general rule of thumb is to make it 6-10 times the width of the line and 5 times the thickness of the substrate [61].
The next step is to set up the spatial discretization of the model, known as the meshing. This dictates how small volumetric pieces our model is split up into, in which the EM-field are discretely solved for. It is important to use a fine enough mesh so that all the physical details of our model can be accurately simulated (i.e. high enough resolution). For a model with only rectangular and square edges (which applies to everything in this thesis except for the casing), everything can accurately be broken down into rectangular mesh cells. CST MWS allows us to set up a finer mesh close to important model details, where the EM-fields will have sharp transitions, and a coarser mesh further away, where there are just a homogeneous medium.
When using the time domain solver, the input waveguide port of our model is excited with a gaussian pulse (shown in figure 6.2). Depending of the selected frequency range, a discrete time step is selected. For each time step, the propagating field is calculated in each individual mesh cell. This continues until the signal energy remaining in the model decays to a pre set energy level. The collected time domain data is then passed trough a Fourier transform to generate frequency domain data, such as S-parameters [54].

1. https://www.cst.com/products/cstmws/technicalspecification

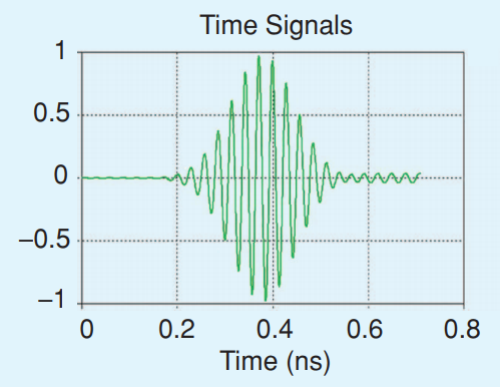

Figure 6.2: A gaussian pulse used to excite the model in the time domain. Reprinted from [61]

6.1.1 Numerical simulation output data

Numerical simulations are used in this thesis to generate reference data. By simulating the sensor in both air and a medium with precisely controllable dielectric properties, we can generate a set of data of the same type, and over the same frequency range, as the expected snow sensor data. This gives us an idealized representation of the sensor data, where the dielectric constant is stepped accurately without changes in the background conditions. The simulation data is not necessarily perfectly accurate in terms of absolute measurements, as that would require us to model all real world imperfections. It should however, represent relative changes to snow dielectric properties very accurate (e.g. how much does the resonance frequency move, for a given change in ϵ_r').

In the plot below (figure 6.3), an example of the simulated data is shown. This particular plot show the transmission response of the snow sensor in air. In other words, the signal at port 2, when signal power is injected into port one. This is how all numerical and experimental data is collected from the probe used in this thesis.
In the plot below, four distinct peaks are visible. The first one at about 700 MHz, the second at about 1.4 GHz, the third at about 2.1 GHz while the fourth is located around 2.7 GHz. These are resonance peaks, meaning frequencies where the snow probe is at resonance. Peak number 1, 2 and 3 are present throughout all gathered data for this thesis, so these are the peaks of interest. By studying the resonance frequencies closer, it is clear that peak 2,3 and 4 are at frequencies approximately equal to multiples of the frequency of the first peak. This makes sense, as the resonance behaviour depends on physical dimensions in the probe. If a given wavelength λ produce produce a standing

wave pattern in the probe (i.e. resonance), so will also 1/2 λ and 1/3 λ.

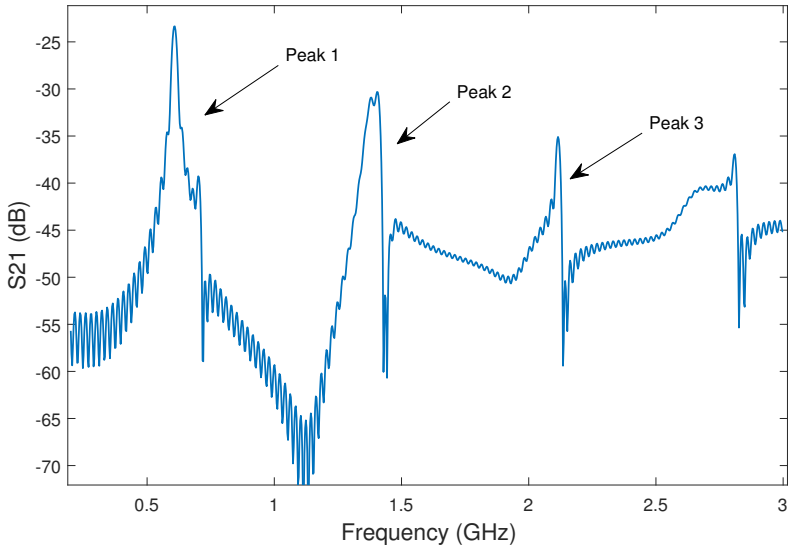

Figure 6.3: Example S21 plot from numerical simulations

The three resonance peaks are visible in most of the results found in this thesis. However, the second peak, located around 1.4 GHz, is the most consistent. It is therefore chosen as the main source of information when analyzing the results. The main parameters that will be recorded are the magnitude, center frequency and the -3 dB bandwidth of this peak. When this data is collected from the numerical simulations, it can be directly compared to the experimental data.

7

In situ measurement techniques

Experimental measurements can be performed in two ways; either from a distance using remote sensing techniques (camera, radar, microphone etc.) or *in situ* (latin phrase measing "on site"). *In situ* refers to making a measurement at the point of interest. It could be on the surface of the sample, or inside of the sample [39].

7.1 Snow probe measurements

The goal of the experimental measurements in this thesis is not to describe the snow *per se*. It is the behaviour of the snow sensor we are interested in, but to achieve that the sensor must be tested in real snow. It is not possible to describe the response of the probe with a single measurement. A range of measurements that is done in snow with varying conditions are needed. In order to produce good experimental results, each single measurement must be performed in a systematic manner.
In order to get appropriate variation in the measurements, the samples were taken vertical down trough the snowpack. This is the same way it is done to determine the distribution of layers in the snow, known as stratigraphy [40]. As the snowpack increases in height due to snowfall, the lower layers will be

slightly compressed, and the density will increase. By measuring both dielectric response, and the density throughout the thickness of the snowpack, we can hopefully characterize the relation between the sensor measurements and the density of the snow.
In the same way as the numerical simulation plot shown in figure 6.3, the snow sensor also output a spectrum containing multiple resonance peaks. The center resonance peak will be studied for each single measurement, and changes in the resonance frequency, magnitude and bandwidth will be studied later.

7.2 Density measurements

The theoretical relation between the real part of the dielectric constant of snow, and the density, is described in chapter 4. From that, it is evident that we should expect at clear connection between the unknown ϵ_r' in the snowpack, and the density. This makes it very useful to measure the density of the snow, at the same location as we perform measurements with the snow probe. We can then correlate the results at a later stage.
A number of methods for determining snow density have been developed, some of them fairly advanced. An intercomparison between existing methods is published in [44]. The density of snow can however be measured without the use of specialized equipment. All that is needed is to determine the weight of a snow sample of known volume, as density ρ, is equal to weight divided by volume. For repeated measurements however, it is advantageous to make a more systematic approach. Personnel which regularly work with determining the density in snow use purpose built density cutters. They are nothing more than a sturdy container, with a known volume. A sample is cut out of a porous material (such as snow), and the sample is weighed. Then the density is calculated. In the figure below, a variety of density cutters is shown.

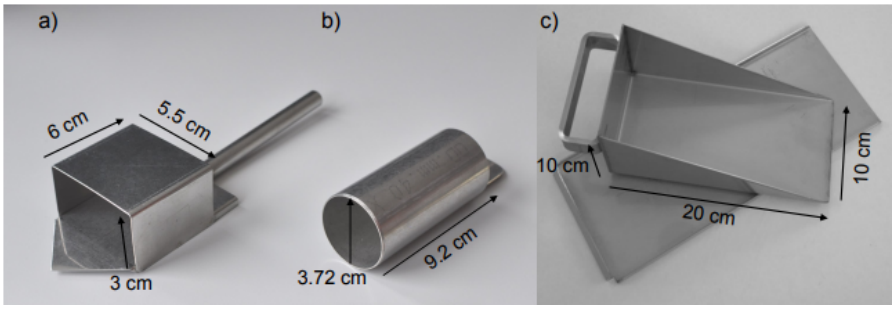

Figure 7.1: Examples of density cutters, box type, tube type and wedge type. Reprinted from [44].

In this thesis, a similar approach was used. For the first field experimental campaign a wooden box was modified by removing one side. It was then used by pushing it into the snowpack, and weighing the content. A model of this box is shown below in figure 7.2. While this method was usable to calculate the density, it suffered from multiple flaws. The most apparent was that the sides of the box where not very sturdy, and tended to bow inwards when it was pressed into the snowpack. This made for inaccuracies in the calculated density. Secondly it requires a rather large sample of material in order to calculate the density. This gives poor spatial resolution, and it is more prone to local variations in density, than a smaller one. A third disadvantage is that this is a destructive way to test for density, so any dielectric measurements must be performed in advance.
In the second field experimental campaign, a PVC tube was used to cut a snow profile, which then was weighed. A model of this cylinder is also shown in figure 7.2. This proved to be a better solution than the box with one side cut away. Due to the round shape of the tube, it did not deform when pressed into the snow. Ideally the diameter of the cylinder would have been smaller, as it would have allowed finer spatial resolution. This would be possible by making more measurements in a given height of the snowpack profile.

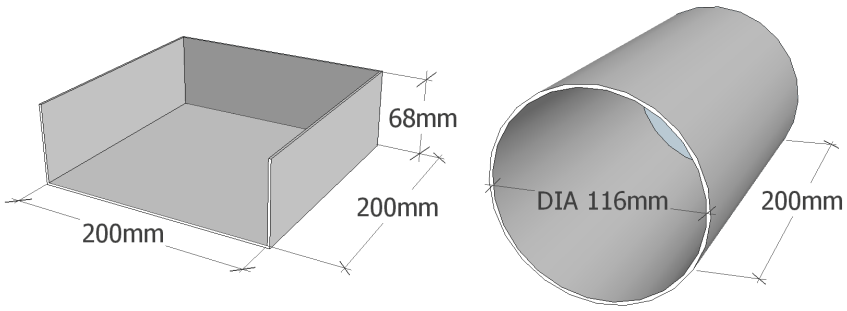

(a) Box

(b) Cylinder

Figure 7.2: CAD rendering of the makeshift density cutters used in this thesis.

7.3 Liquid Water measurements

There exist a number of techniques for measuring the free water content in snow. Kuroda and Hurukawa used centrifugal separation [30], Yosida used melting calorimetry [64] and Jones et al. and others have used freezing calorimetry [27]. A review of available methods for snow water measurements was published by Stein et al. [50]. Common for all these methods is that they are difficult to perform and time consuming. The freezing calorimeter method, which

appears to be the most used method throughout the literature, requires an insulated bottle, a freezing agent and an accurate thermometer. A snow sample is placed in the insulated bottle, and the freezing agent is added. The amount of heat gained by the mixture is then measured, and used to calculate the amount of water that froze in the process. As the amount of water in the snow sample is small compared to the amount of freezing agent, all the free water is assumed to freeze. This technique is accurate within ± 1.0-2.0 % by weight (about ± 0.5% by volume) [27], however, because of the complex procedure, it is not practical to use for operational forecasting [55]. When Swiss avalanche professionals investigate avalanche risk, liquid water content is typically estimated by conducting hand tests throughout the layers of the snowpack [17]. A detailed description of such a hand test is given in table 7.1, shown below.

Table 7.1: Description of a hand test used for qualitatively estimating the liquid water content (mWC) , and the approximate range of water content θ. t_s is the snow temperature. Reproduced from [55].

Wetness Content	Index (mWC)	Description	θ [vol. %]
Dry	1	t_s sec 0.0°C. Disaggregated snow grains have little tendency to adhere to each other when pressed together.	0
Moist	2	$t_s = 0.0°C$. The water is not visible, even at 10× magnification. When lightly crushed, the snow has a tendency to stick together.	0-3
Wet	3	$t_s = 0.0°C$. The water can be recognized at 10× magnification by its meniscus between adjacent snow grains, but water cannot be pressed out by moderately squeezing the snow in the hands.	3-8
Very Wet	4	$t_s = 0.0°C$. The water can be pressed out by moderately squeezing the snow in the hands, but an appreciable amount of air is confined within the pores.	8-15
Soaked	5	$t_s = 0.0°C$. The snow is soaked with water and contains a volume fraction of air from 20 to 40 %.	>15

When performing the hand test described above, a snow sample is squeezed with your hand, and the response by the snow is evaluated according to the

table. This method obviously require a certain degree of experience of the operator, and even for a skilled snow avalanche professional it will still be up to his or hers subjective opinion. The water volume content θ for each index is given in ranges, and therefore only gives a rough estimation. However, the accuracy of the estimated ranges is found to be good, but errors are introduced as the water content exceed 8 vol. % [55].

In order to fully characterize the response of the snow sensor, it must be thoroughly tested in all types of snow, including both wet and dry snow. Every sensor measurement should have a corresponding measurement of density and wetness. This way we can establish an empirical relation between S21-plots measured by the sensor, and the density and the wetness in the snowpack. However, the wetness of the snowpack is season dependent. Wet snow is typically present in northern Norway when the snow is melting during the spring season, or it could be introduced by rainwater. The two experimental campaigns carried out for this thesis was done in periods with dry weather and temperatures below freezing. The experimental measurements could therefore unfortunately only be conducted in dry snow.
In order to establish a capability to measure water content with this sensor, additional experimental work is needed. Measurements done in snow with varying degree of wetness should be performed, preferably during the spring season, when wet snow is readily available in the northern part of Norway.

Part III

Results

8

Quasi analytical approximations of the resonance frequency

8.1 Solving for air medium

A quasi analytical expression for calculating the resonance frequency in terms of substrate and superstrate dielectric constants was presented in section 3.2. In the present section we will use the expressions to solve for the resonance frequency in terms of the dielectric constant of snow acting as a superstrate on a microstrip.
We input the physical dimensions given in section 5.1. To calculate resonance frequency in air, we use $\epsilon_r' = 1.0$. Superstrate thickness is not relevant when the superstrate is air, and is therefore set to an arbitrary large value of 1 metre. This gives us a result of the first resonance peak, f_1 at 706.8 MHz. As we know from section 6.1.1, the 2nd and 3rd resonance peak fall on frequencies that are multiples of f_1. We therefore get $f_2 = 1.413$ GHz and $f_3 = 2.120$ GHz, where f_2 is the main frequency of interest.

8.2 Solving for snow superstrate resonance frequency

We apply the same quasi analytical model as above, but this time with superstrate dielectric constant values equal to what is typically found in snow. We start with a value of $\epsilon_r' = 1.1$. Values are then calculated with 0.05 increments up to 1.4, to match the dielectric constant of dry snow of very low density. Some further resonance frequency is calculated with a dielctric constant of 1.6, 1.8 and 2.0. The resulting resonance frequencies are plotted in figure 8.1.

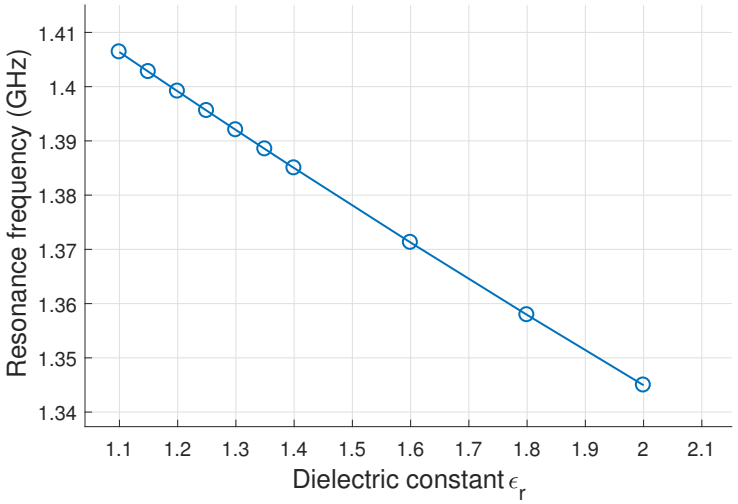

Figure 8.1: Quasi analytical approximation of resonance frequency, solved in terms of snow superstrate dielectric constant

We observe that the calculated resonance frequencies lie on an almost straight line, with increasing values for ϵ_r' resulting in a lower resonant frequency. A 0.05 change in dielectric constant gives around a 3.55 MHz change in resonance frequency, while a 0.2 change in dielectric constant results in a change of 13 MHz change. However, the amount of shift decreases as ϵ_r' gets larger.

9 Numerical simulations

9.1 Numerical simulations of the sensor in air

Numerical simulations have been run on the snow sensor system. The results from simulating the sensor in both air, and dielectric media representing snow, will be presented in this section. The simulation software does not make it possible to simulate the inhomogeneous nature of snow such as varying particle size and possible water or ice inclusions. The snow is therefore simulated as a homogeneous material, with dielectric properties matching the effective dielectric properties commonly found for snow [46]. As the experimental data collected for this thesis only were conducted in dry snow, the numerical models will try to match the dielectric properties of dry snow. Doing so, the simulations are conducted by varying the real part of the dielectric constant ϵ_r' and keeping the complex part ϵ_r'' constant. In this way, each simulation will give results similar to dry snow of varying density, and will be better suited for direct comparison with the experimental results.

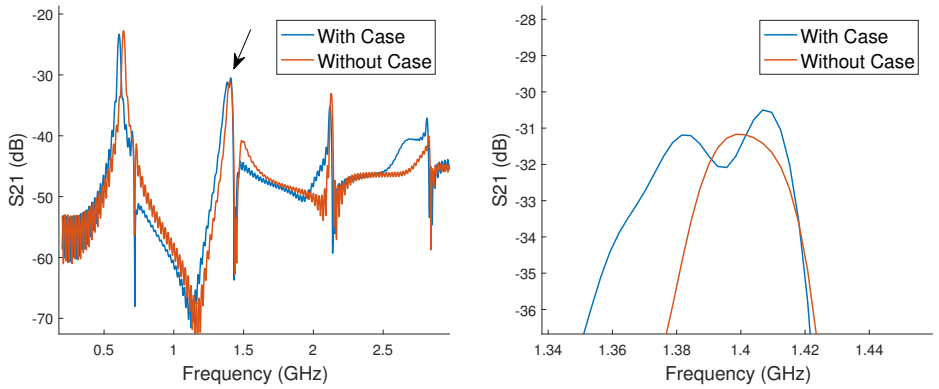

(a) Full plot **(b)** Zoomed at peak 2

Figure 9.1: S21 plot from simulations with and without 3D-printed case

Some simulations were run to get the settings right. The final simulation series is run with ϵ_r' ranging from 1.1 to 1.8, in steps of 0.05 at low values of ϵ_r', and steps of 0.2 at higher values of ϵ_r', and with the complex ϵ_r'' at a constant 0.045. This way the changes in the results are due to changes in the real part of the dielectric constant, as well as small changes in the loss tangent $\tan\delta = \epsilon_r''/\epsilon_r'$, due to the changes in ϵ_r'. The idea behind this simulation setup is to simulate dry snow with changing density, as there is an expected strong relation between dry snow density and ϵ_r'.
The above plot in figure 9.1 shows the output from two simulation runs (in air), with and without the 3D-printed case included in the model. The simulation settings were identical apart from simulating with and without case. We observe that when the simulation includes the 3D-printed case in the model, peak number 2 is split into two overlapping peaks. As we want to measure changes in the resonance frequency, in order to determine the dielectric constant, it is important to reveal possible sources of error in the measurement setup. As the plot shows, it would have been difficult to determine the center frequency of the double peak. There is also a bandwidth discrepancy of about 25 MHz between the two plots.

The resonance frequency of the probe simulated in air (shown in figure 9.1) is 1.402 GHz.

9.2 Numerical simulations for snow media

From the results of the numerical simulations, we are primarily interested in the resonance frequency of each separate run. The numerical model is an idealized model, where the only change between each run is the dielectric constant in the medium. This way we get a relation between resonance frequency and dielectric constant.

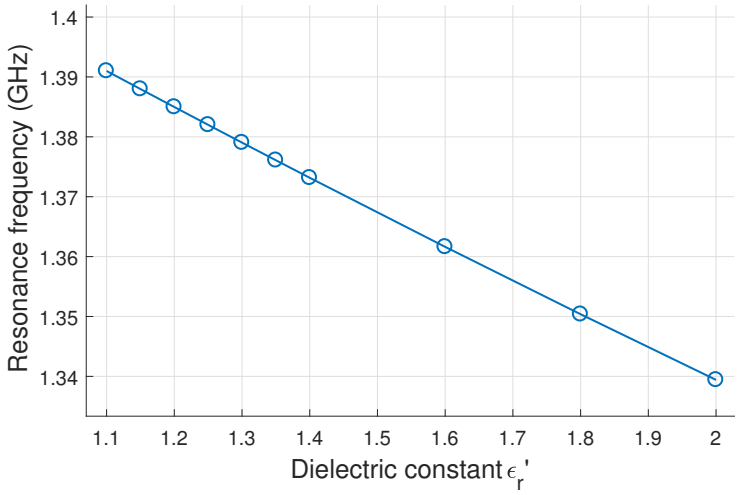

Figure 9.2: Resonance frequencies in the results generated by the numerical simulations. Plotted against the real part of the dielectric constant.

In figure 9.2, the resonance frequency is plotted as a function of dielectric constant. As can be expected, when only varying the dielectric constant, the results show consistently spaced resonance frequencies. The change in resonance frequency, due to a 0.05 change in the dielectric constant is 3 MHz, while a 0.2 change in dielectric constant give a change in resonance frequency of about 10 MHz. We can compare these numbers to the change in resonance frequency we measure in real snow.

Other features in the snow simulations

The resonance frequency is the main parameter of interest, because it directly relates to the dielectric constant in dry snow. However, it is not the only part of the measured resonance spectrum that contain information about the medium. From section 3.1, we know that the amplitude, and the bandwidth of the resonance peak describe how a resonator stores energy. A low and wide peak corresponds to more energy loss than a narrow, energetic peak. By measuring the bandwidth and the peak amplitude of the resonance peak, we can extract some useful information about the loss in the measured system.

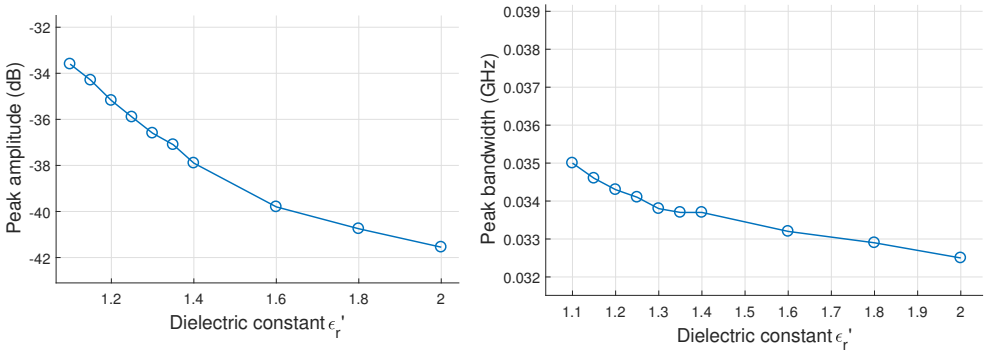

(a) Peak amplitude vs. ϵ_r'

(b) Peak bandwidth vs. ϵ_r'

Figure 9.3: Peak amplitude and peak bandwidth plotted as a function of simulated ϵ_r'

The plot in figure 9.3, shows changes in peak amplitude, and peak bandwidth found by the simulations. From the plot of peak bandwidth, it is clear that an increased dielectric constant, does not change the bandwidth. This is expected, as an increased bandwidth would be the result of more loss in the medium. As the simulations were run with the complex dielectric constant ϵ_r'' equal to 0.045 for all simulations, there should be equal losses for all simulations. As for the decrease in peak amplitude, this is likely due to limitations in the time domain solver used for the numerical simulations. The discretized nature of the model, with a finite number of mesh cells, makes it difficult to compute narrow bandwidth resonance phenomenons very accurately. To remedy this, an get more accurate simulations of resonant systems, there also exist a separate resonance solver in CST studios. However, this was not utilized in this thesis, as the position of the peaks are the main source of information.

10

In situ measurements

The experimental measurements in snow were conducted on two separate days in November and December 2017. Both days of measuring were conducted after a recent snowfall in the Tromsdalen area of Tromsø. Below is a photograph of the snowpit where the second set of measurements were conducted.

Figure 10.1: Photograph of the snow profile at 06/12, with round density profile cuts shown.

The density cutting equipment used for the measurements on 01/11 was a box with sides measuring 6.8×20×20 cm^3. This gives a total measurement volume of 2720 cm^3. However, the sides of the box suffered from deflection when pushed into the snow. This caused a significant uncertainty estimated to be around 200 cm^3. The volume used for calculating the density was therefore 2620 cm^3 ± 100 cm^3. A regular kitchen scale was used for weighing the samples. The resolution of the scale is 0.1 grams and it has a given uncertainty of ± 1g. For the measurements conducted 06/12 an improved approach for measuring density was used. A PVC tube with a length of 20 cm and an inside diameter of 11.6 cm was used. This gives a measured volume of 2114 cm^3. The tube did not suffer from deflection when retrieving a sample, however, a slight amount of snow would typically fall out of the sample tube when it was extracted from the snowpack. Taking this into account, we get an estimated measurement volume of 2100 cm^3 ± 30 cm^3. The same kitchen scale was used on both days.

10.1 *In situ* measurements 1/11

The thickness of the snowpack at 1/11 was 46 cm, where everything except the bottom 4 cm was recently fallen snow. In this snowpack, three vertically separated density measurements were taken. This low number is mainly due to a less than ideal method for extracting the snow sample. The resulting density values are shown in table 10.1.

Table 10.1: Measured density in the snowpack at 1/11/2017

Sample depth (cm)	Density (g/cm^3)
3.5	0.0870 ± 4 %
27	0.1504 ± 4 %
41	0.1698 ± 4 %

With the probe, the resonance frequency in air was measured to 1.4112 GHz. Then a series of six measurement were conducted vertically trough the snowpack. The measured resonance frequency is shown below in figure 10.4.

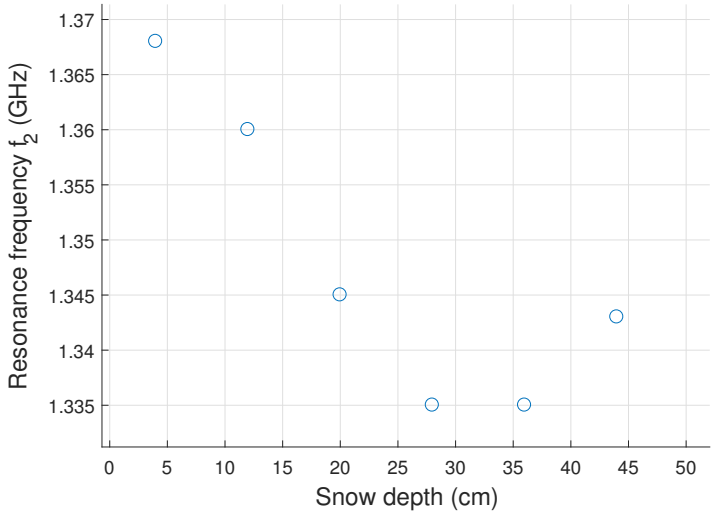

Figure 10.2: Resonance frequency measured vertically trough the snowpack.

By studying the above plot we observe a declining resonance frequency down trough the first 30 cm of the snowpack. However, the last two measurements show an increase in resonance frequency. A possible explanation could be movement in the inserted probe, which created an air pocket around the sensor prongs, and thereby throwing the result off. This was however not further investigated, as the results were analysed at a later time.

10.2 *In situ* measurements 6/12

Density measurements
The thickness of the snowpack was measured to be 68 cm, and the density was measured in two vertical series of 4 depths each.

Table 10.2: Snow density, measured 6/12/2017

Depth (cm)	Density left (g/cm^3)	Depth (cm)	Density right (g/cm^3)
6.0	0.079 ± 1%	4.5	0.075 ± 1%
21.1	0.090 ± 1%	21.8	0.088 ± 1%
36.0	0.103 ± 1%	32.9	0.113 ± 1%
47.0	0.203 ± 1%	50.7	0.162 ± 1%

The density measurements shown in table 10.2 were measured vertically, in two series. The density measurement done at depth 47 cm in the left series contained ice in the back of the cut profile. This has likely caused an inflated density value for this measurement. For the plot of the density values (shown in figure 10.3), this measurement is marked by an arrow.
The density values at the depth of each measurement is fitted using a polynomial regressive model, based on the measured densities. It is calculated by the basic fitting tool in MATLAB. The model is a second order polynomial, fitted to the known density measurements, and it is given by:

$$\rho(y) = 4.2 \times 10^{-5}\, y^2 - 5.4 \times 10^{-4}\, y + 0.079$$

where y is the measurement depth in the snowpack in centimetres, and ρ is the calculated density. The inconsistent measurement was discarded before calculating the polynomial model.

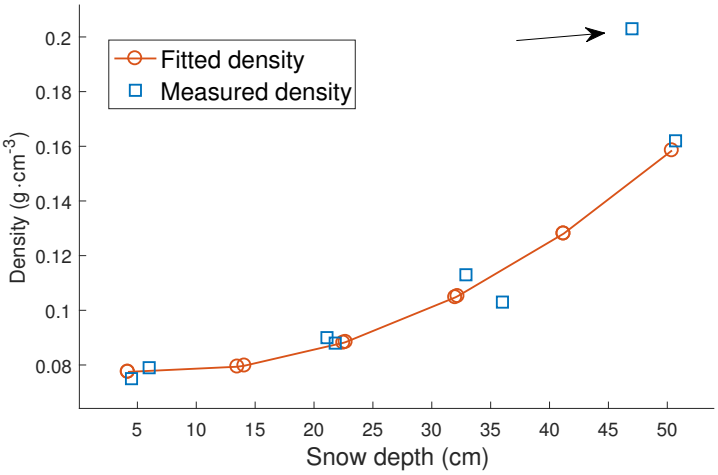

Figure 10.3: Measured density and density at the measurement depth, fitted by a 2nd order polynomial model.

Measuring the resonance frequency

The most important parameter we measure is the resonance frequency. By measuring the shift in resonance frequency from air to snow, across a range of snow densities, we can establish a correlation between air-snow shift, and the density. We know from section 3.2 that an increase in density will cause a decrease in resonance frequency.

Two sets of measurements were conducted (at 6/12) with the snow probe. The first measurement series was conducted at the left side of the density profiles, and the other series on the right side. Both series contained 6 individual measurements, vertically down trough the snowpack. The spacing between each measurement was 9 cm.

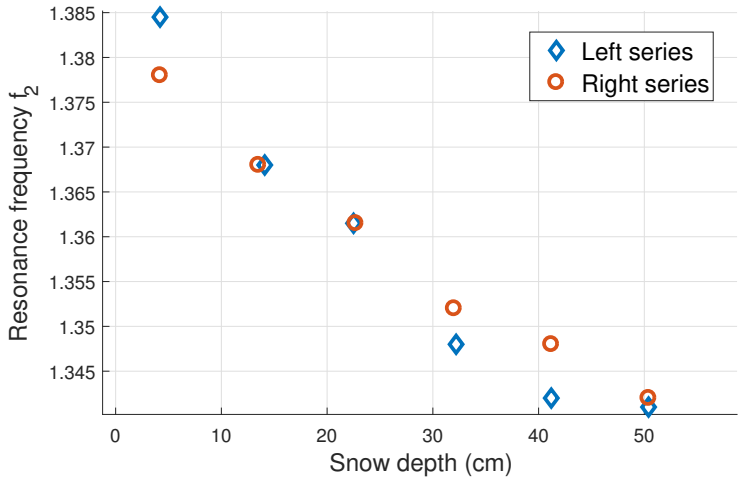

Figure 10.4: Resonance frequency measured vertically trough the snowpack, in two series.

In figre 10.4, the measured resonance frequency is plotted versus the depth of the measurements in figure 10.4. It is clear from the plot that the resonance frequency decreases, as the measurements get deeper in the snowpack. This is expected, as the snow density measurements showed increasing density values down trough the snowpack.
Hence, this is a good indication that the snow sensor is able to detect an increase in density of dry snow. In a later section, we will compare the results presented in this section to the numerical results, and results published in the literature.

Measuring other features

Just as we did in section 9.2, we also include the peak amplitude and the bandwidth of the resonance peaks in the results. These measurements are another source of information, not directly related to the dielectric constant in the medium.

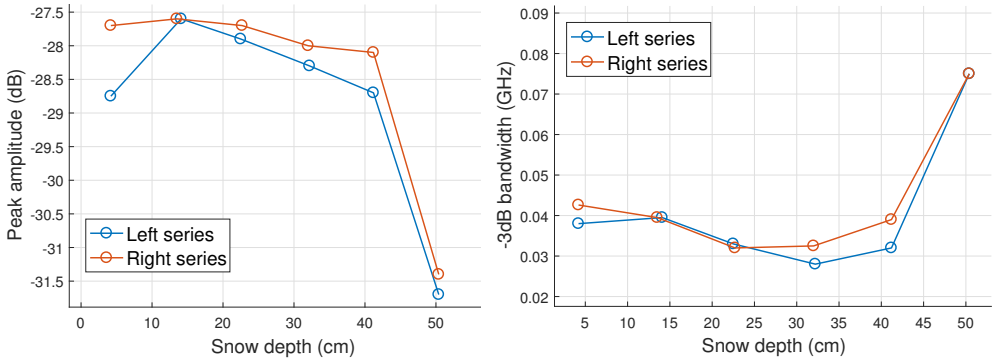

(a) Peak amplitude vs. snow depth **(b)** Peak bandwidth vs. snow depth

Figure 10.5: Peak amplitude and peak bandwidth plotted as a function of depth of measurement in the snowpack.

In figure 10.5, the measured peak amplitude and bandwidth are plotted versus snow depths. The plot shows that both the amplitude and bandwidth only have small changes at shallow snow depths. However, for the measurements done at the bottom of the snowpack there is a large change, a decrease of about 3 dB peak amplitude and a bandwidth increase of about 35 MHz. Without drawing substantial conclusions, we can say that these results indicate a fairly constant loss factor trough the snowpack, with the exception of the very bottom. This is likely caused by an increased content of ice, and other contaminations near the surface of the ground. When the snow pit was dug, we observed a thin boundary layer between the ground and the snowpack, made up of old densely packed snow, ice and grass.

11

Comparing results

In chapter 8, 9 and 10, results from quasi analytical models, numerical simulations and *in situ* measurements are presented. In this chapter we want to compare the results.

11.1 Correlation between analytical model, simulations and *in situ measurements*

We established in section 4.1, that for dry snow, the real part of the dielectric constant, ϵ_r', have an almost linear dependence on the density in the snow. The empirical relation presented in equation (4.1) is used to calculate the real part of the dielectric constant, from the density of the snow samples. The measured resonance frequency can then be plotted against the calculated dielectric constant in the *in situ* measurement data. This makes it possible to directly compare the data from the quasi-analytical model, numerical simulations and *in situ* measurements. In figure 11.1, the resonance frequency is plotted directly versus the dielectric constant.

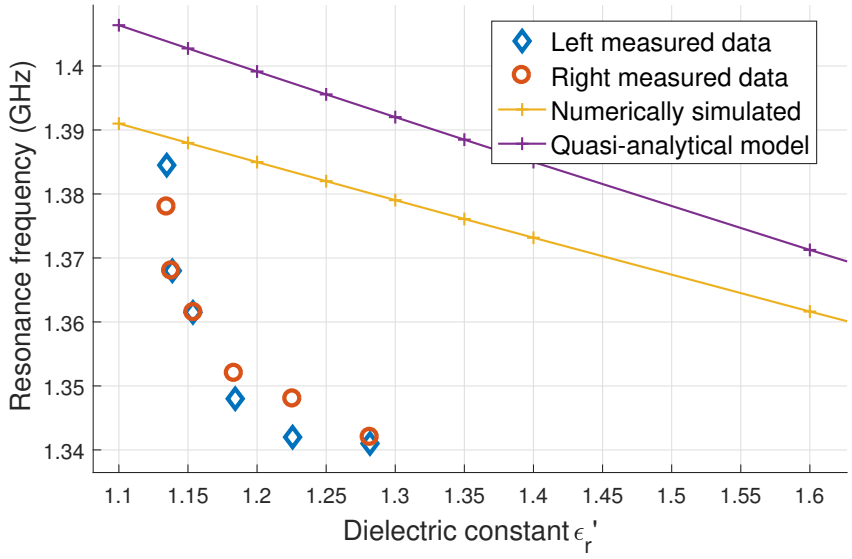

Figure 11.1: Resonance frequency calculated by the quasi analytical model, simulated numerically and from *in situ* measurements plotted against the dielectric constant

It is clear in figure 11.1, that the results from the quasi analytical model, and the numerically simulated results follows a similar slope. There is a discrepancy between the two of between 10-15 MHz with values for ϵ_r' ranging from 0.1 to 1.8. The increased resonance frequency from the analytic model is likely due to small inaccuracies in the model. The amount of error between the two lies between 1.2% at low values of ϵ_r' and 0.5% at the higher values of ϵ_r'.
The *in situ* measurements shows a discrepancy from the numerically and analytically expected values. In figure 11.1, the discrepancy increase as the corresponding dielectric constant increase. The relative errors in figure 11.1 is presented in table 11.1.

Table 11.1: Relative errors between measured resonance frequency and numerically simulated resonance frequency.

ϵ_r'	Error left data (%)	Error right data (%)
1.135	0.3	0.8
1.138	1.5	1.5
1.154	1.9	1.9
1.183	2.7	2.5
1.226	3.0	2.6
1.282	2.8	2.8

Normalized resonance frequency

The dielectric constant in the snowpack is the unknown parameter we want to measure. As the dielectric constant of air has a constant value, $\epsilon_r \approx 1$, we want to relate the measured resonance frequency in snow, to the resonance frequency in air. We therefore normalize the snow resonance frequency in snow with respect to the resonance frequency in air. This is similar to how it is done by the Snow Fork developed by Tiuri et al. [46]:

$$f_{norm} = \left(\frac{f_{air}}{f_{snow}} \right)^2 .$$

In figure 11.2, the normalized resonance frequencies are plotted versus the dielectric constant. Normalized resonance frequency from the analytical and numerical data is plotted along side the *in situ* data for comparison.

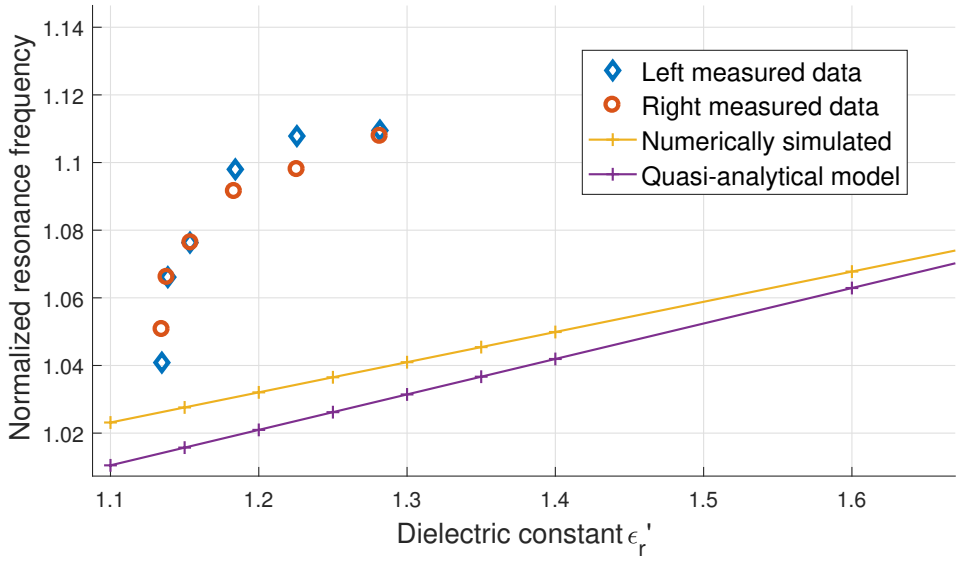

Figure 11.2: Normalized resonance frequency calculated by the quasi analytical model, simulated numerically and from *in situ* measurements plotted against the dielectric constant

Figure 11.2 shows a similar situation as figure 11.1. The quasi-analytical model and the numerical data has a discrepancy of 1.2 % at the lower values of ϵ_r' which decreases towards zero when ϵ_r' increase. For the *in situ* data, the relative error is increased in the normalized resonance frequency data. This is because the resonance frequency measured in air with the snow sensor are slightly higher than the air resonance frequency from the simulations. The relative errors in figure 11.2 are presented in table 11.2.

Table 11.2: Relative errors in the measured normalized resonance frequencies.

ϵ_r'	Error left data (%)	Error right data (%)
1.135	1.5	2.4
1.138	3.8	3.8
1.154	4.6	4.6
1.183	6.5	5.9
1.226	7.2	6.2
1.282	6.7	6.6

Part IV

Conclusion & Discussion

12

Discussions

In the present chapter the results presented in Part III will be discussed. A number of results were presented in Part III, however, the main goal in this thesis was to figure out if this sensor design was useful, and to describe the sensors ability to measure the dielectric constant of snow.

Numerical simulations Numerical simulations run within CST studio is a very powerful tool to create realistic simulations of the response of the snow sensor in both air and snow. These simulations have been used as a comparative reference of how the sensor was expected to behave in snow of varying density.

In situ measurements

In situ measurements with the snow sensor were conducted on two separate days in the end of the fall semester 2017. The measurements done on 1/11 was the first test of the sensor system in actual snow. A procedure for conducting repeated measurements had to be established. Some preliminary tests of the response in snow were tried out before conducting a proper measurement series. The density measurements conducted on 1/11 where unfortunately not very accurate, and the density was also measured with to low vertical precision. Ideally both the density and the snow probe measurements should have been conducted more than once trough a vertical snowpack profile. Then the correlation between multiple series could have been investigated. However, the

results down until about 30 cm deep into the snowpack shows that the sensor responds with a decrease in resonance frequency, when the density increases. The inconsistent results at the very bottom of the snowpack is likely caused by some mechanical properties of the boundary layer between the ground and the snowpack. This could be grass, dirt or possibly larger pieces of ice.

For the measurements 06/12, an improved approach to the measurement procedure was taken. A much more useful method for measuring the density was used. This allowed better accuracy, and slightly more measurements trough the vertical snow profile. This time two sets of density measurements were conducted, to allow comparison between them. Ideally, an even smaller cylinder would be used to conduct the density measurements. Together with a scale with higher accuracy, the density could have been measured on more depths trough the snow pack. A better empirical relation between snow density and resonance frequency could then have been established.
Initially, the plan was to use a Toikka Snow fork (as mentioned in section 1.3) to conduct comparative measurements of both density and dielectric constant. However, it proved to be impossible to get hold of such an instrument during the measurement campaigns.

Correlation between measurements and reference data When directly comparing the data from the analytical model and numerical simulations to the *in situ* measurements, it is evident that they do not line up perfectly. This is shown in figure 11.1 and 11.2. When comparing the absolute resonance frequency from the *in situ* measurements with the reference data, an error ranging from 0.3 to 3% is observed. This is a reasonable low error, but it is worse than what can be expected from existing instruments (e.g. the Snow Fork [46]). When normalizing the resonance frequency in snow to the resonance frequency in air, the errors range from 1.5 to 7.2%.

13

Conclusions

In this thesis we have tested a resonance snow probe system, and its capability to measure the dielectric constant in snow. The results presented in Part III, show that changes in the density of the snow is measurable by the sensor in the form of a change in resonance frequency. Furthermore does the sensor system show a reduced resonance frequency as the density (and implicitly ϵ_r') increase, as predicted by the theory and numerical simulations.
In chapter 11, the results from quasi analytical approximations, numerical simulations and *in situ* measurements were compared. Relative errors for measured absolute resonance frequency and normalized resonance frequency are in a range of 0.3% to 3% and 1.5% to 7.2% respectively.

13.1 Future work

In order to establish a more robust empirical model for calculating the dielectric constant with resonance measurements from the snow probe, more *in situ* measurements must be conducted. Especially important is to test the response in seasonal snow, of varying age and with varying grain structure. Seasonal snow will also have free water inclusions. In order to characterize the sensor response in snow containing free liquid water, a good system for measuring the free water content is needed.

Data post processing

Reading parameters such as resonance frequency and peak bandwidth from the measured resonance spectrum is not straight forward. The measurements are jagged and noisy, and a more robust method for extracting resonance frequency and bandwidth would be very advantageous.

Asymmetric resonance curves are appearing in the measured data, and a Fano resonance model could potentially be fitted to the measured data. This could make the sensor system capable of extracting more information about the snowpack, suck as information about the structure and particle sized in the snow. However, this would require significant research on Fano resonance effects in snow.

Integrated solution

The MiniVNA network analyser comes with a command line interface which run only requires Java. This could be utilized to create an integrated, self contained unit without the need of a laptop computer or a cellphone. Small single board computers are available today, which supports Java, and are powerful enough to perform automated acquisition, and post processing of data. This could become an all-in-one solution able to measure and display the dielectric constant in a very compact and portable package.

Bibliography

[1] W Ambach and A Denoth. On the dielectric constant of wet snow. *IAHS-AISH Publ*, 114:136–142, 1975.

[2] Andrei Andryieuski, Svetlana M Kuznetsova, Sergei V Zhukovsky, Yuri S Kivshar, and Andrei V Lavrinenko. Water: Promising opportunities for tunable all-dielectric electromagnetic metamaterials. *Scientific reports*, 5, 2015.

[3] Peter Atkins and Julio de Paula. *Physical Chemistry, 9th Edition*. W. H. Freeman, 2009.

[4] I. Bahl, P. Bhartia, and S. Stuchly. Design of microstrip antennas covered with a dielectric layer. *IEEE Transactions on Antennas and Propagation*, 30(2):314–318, Mar 1982.

[5] I Bahl, Prakash Bhartia, and S Stuchly. Design of microstrip antennas covered with a dielectric layer. *IEEE Transactions on Antennas and Propagation*, 30(2):314–318, 1982.

[6] Tim P Barnett, Jennifer C Adam, and Dennis P Lettenmaier. Potential impacts of a warming climate on water availability in snow-dominated regions. *Nature*, 438(7066):303–309, 2005.

[7] C. Caloz and T. Itoh. *Electromagnetic Metamaterials: Transmission Line Theory and Microwave Applications*. Wiley - IEEE. Wiley, 2005.

[8] Flynn Castles, Dmitry Isakov, A Lui, Q Lei, CEJ Dancer, Y Wang, JM Janurudin, SC Speller, CRM Grovenor, and Patrick S Grant. Microwave dielectric characterisation of 3d-printed batio3/abs polymer composites. *Scientific reports*, 6:22714, 2016.

[9] L. F. Chen, C. K. Ong, C. P. Neo, V. V. Varadan, and Vijay K. Varadan. *Microwave Electronics: Measurement and Materials Characterization*. Wiley, 2004.

[10] SC Colbeck. The geometry and permittivity of snow at high frequencies. *Journal of Applied Physics*, 53(6):4495–4500, 1982.

[11] Rogers Coorporation. Ro4000 data sheet. `http://www.rogerscorp.com/documents/726/acs/RO4000-LaminatesData-Sheet.pdf`, 2017. original document from Rogers Coorporation.

[12] WA Cumming. The dielectric properties of ice and snow at 3.2 centimeters. *Journal of Applied Physics*, 23(7):768–773, 1952.

[13] Andreas Juergen Dietz, Claudia Kuenzer, Ursula Gessner, and Stefan Dech. Remote sensing of snow – a review of available methods. *International Journal of Remote Sensing*, 33(13):4094–4134, 2012.

[14] MC Dobson and R Austin. In situ determination of snow density and wetness using microwave dielectric probes. In *Geoscience and Remote Sensing Symposium, 1989. IGARSS'89. 12th Canadian Symposium on Remote Sensing., 1989 International*, volume 3, pages 1256–1256. IEEE, 1989.

[15] S Evans. Dielectric properties of ice and snow–a review. *Journal of Glaciology*, 5(42):773–792, 1965.

[16] Ugo Fano. Effects of configuration interaction on intensities and phase shifts. *Physical Review*, 124(6):1866, 1961.

[17] C Fierz and PMB Föhn. Long-term observation of the water content of an alpine snowpack. In *Proceedings International Snow Science Workshop, Snowbird, Utah, USA*, volume 30, pages 117–131, 1994.

[18] Michel Fily, Jean-Pierre Dedieu, and Sylviane Surdyk. A sar image study of a snow-covered area in the french alps. *Remote sensing of environment*, 51(2):253–262, 1995.

[19] Douglas Giancoli. *Physics : principles with applications*. Pearson/Prentice Hall, Upper Saddle River, N.J, 2005.

[20] David Griffiths. *Introduction to electrodynamics*. Pearson, Boston, 2013.

[21] Martti T Hallikainen. Microwave radiometry of snow. *Advances in Space Research*, 9(1):267–275, 1989.

[22] Martti T Hallikainen, Fawwaz T Ulaby, and Tahera Emille Van Deventer. Extinction behavior of dry snow in the 18-to 90-ghz range. *IEEE Transactions on Geoscience and Remote Sensing*, GE-25(6):737–745, 1987.

[23] Arne Egil Tønset Helge Carlsen, Emrah Senel. Barn døde etter snøskredet på svalbard. https://www.nrk.no/troms/barn-dode-etter-snoskredet-pa-svalbard-1.12714226, 2015. Retrieved from web page January 15 2018.

[24] Charles L Hosler, DC Jensen, and Leon Goldshlak. On the aggregation of ice crystals to form snow. *Journal of Meteorology*, 14(5):415–420, 1957.

[25] J. V. Hughes and H. L. Armstrong. The dielectric constant of dry air. *Journal of Applied Physics*, 23(5):501–504, 1952.

[26] Yong S Joe, Arkady M Satanin, and Chang Sub Kim. Classical analogy of fano resonances. *Physica Scripta*, 74(2):259, 2006.

[27] EB Jones, A Rango, and SM Howell. Snowpack liquid water determinations using freezing calorimetry. *Hydrology Research*, 14(3):113–126, 1983.

[28] John R Kendra, Fawwaz T Ulaby, and Kamal Sarabandi. Snow probe for in situ determination of wetness and density. *IEEE Transactions on Geoscience and Remote Sensing*, 32(6):1152–1159, 1994.

[29] Raj Kumar and P Malathi. Effects of superstrates on the resonant frequency of rectangular microstrip antennas. *Microwave and optical technology letters*, 49(12):2946–2950, 2007.

[30] Masawo Kuroda and I Hurukawa. Measurement of water content of snow. *IASH Assemblee Generale de Rome*, 39:38–41, 1954.

[31] Daisuke Kuroiwa. *The dielectric property of snow*. International Association of Scientific Hydrology, 1954.

[32] Kenneth G Libbrecht. The physics of snow crystals. *Reports on progress in physics*, 68(4):855, 2005.

[33] C Lobban, JL Finney, and WF Kuhs. The structure of a new phase of ice. *Nature*, 391(6664):268–270, 1998.

[34] Choji Magono. On the growth of snow flake and graupel. *Science Reports of the Yokohama National University*, 2:18–40, 1953.

[35] James H. McClellan, Ronald W. Schafer, and Mark A. Yoder. *Signal Processing First*. Pearson, 2003.

[36] Andrey E Miroshnichenko, Sergej Flach, and Yuri S Kivshar. Fano resonances in nanoscale structures. *Reviews of Modern Physics*, 82(3):2257,

2010.

[37] Philip W. Mote, Alan F. Hamlet, Martyn P. Clark, and Dennis P. Lettenmaier. Declining mountain snowpack in western north america*. *Bulletin of the American Meteorological Society*, 86(1):39–49, 2005.

[38] OMOLARA OLOWOYEYE. Snowflakes. *DARTMOUTH UNDERGRADUATE JOURNAL OF SCIENCE*, 5(2), 2003.

[39] Roger A. Pielke. Atmosphere. `https://www.britannica.com/science/atmosphere/Stratosphere-and-mesosphere`, 2017. Accessed date: 2018-01-26.

[40] Christine Pielmeier and Martin Schneebeli. Developments in the stratigraphy of snow. *Surveys in geophysics*, 24(5):389–416, 2003.

[41] D Polder and JH Van Santeen. The effective permeability of mixtures of solids. *Physica*, 12(5):257–271, 1946.

[42] Df Pozar. Input impedance and mutual coupling of rectangular microstrip antennas. *IEEE Transactions on Antennas and Propagation*, 30(6):1191–1196, 1982.

[43] D.M. Pozar. *Microwave Engineering*. Wiley, 2012.

[44] Martin Proksch, Nick Rutter, Charles Fierz, and Martin Schneebeli. Intercomparison of snow density measurements: bias, precision, and vertical resolution. *The Cryosphere*, 10(1):371–384, 2016.

[45] Reuven Shavit. Dielectric cover effect on rectangular microstrip antenna array. *IEEE Transactions on Antennas and propagation*, 42(8):1180–1184, 1994.

[46] A. Sihvola and M. Tiuri. Snow fork for field determination of the density and wetness profiles of a snow pack. *IEEE Transactions on Geoscience and Remote Sensing*, GE-24(5):717–721, Sept 1986.

[47] Ari H Sihvola and Jin Au Kong. Effective permittivity of dielectric mixtures. *IEEE Transactions on Geoscience and Remote Sensing*, 26(4):420–429, 1988.

[48] Rune Solberg and Tom Andersen. An automatic system for operational snow-cover monitoring in the norwegian mountain regions. In *Geoscience and Remote Sensing Symposium, 1994. IGARSS'94. Surface and Atmospheric Remote Sensing: Technologies, Data Analysis and Interpretation., Interna-*

tional, volume 4, pages 2084–2086. IEEE, 1994.

[49] Mini Radio Solutions. Hardware manual for minivna tiny. http://www.wimo.de/download/MiniVNA_Tiny_hardware-manual_en.pdf, 2014. Accessed date: 2018-01-22.

[50] Jean Stein, Gaetan Laberge, and Denis Lévesque. Monitoring the dry density and the liquid water content of snow using time domain reflectometry (tdr). *Cold Regions Science and Technology*, 25(2):123–136, 1997.

[51] Marc Stieglitz, SJ Déry, VE Romanovsky, and TE Osterkamp. The role of snow cover in the warming of arctic permafrost. *Geophysical Research Letters*, 30(13), 2003.

[52] WH Stiles and FT Ulaby. Dielectric properties of snow. Technical report, DTIC Document, 1980.

[53] S Surdyk and S Fujita. Microwave dielectric properties of snow: Modeling and measurements. *Geophysical research letters*, 22(8):965–968, 1995.

[54] CST team. *Understanding Time Domain Meshing in CST MICROWAVE STUDIO*, July 2010. URL: https://www.researchgate.net/file.PostFileLoader.html?id=578c450ceeae3937441b63a1&assetKey=AS%3A385033333428224%401468810508239.

[55] F. Techel and C. Pielmeier. Point observations of liquid water content in wet snow – investigating methodical, spatial and temporal aspects. *The Cryosphere*, 5(2):405–418, 2011.

[56] Agilent technologies Inc. Agilent fieldfox n9916a datasheet. http://www.testequipmenthq.com/datasheets/Agilent-N9916A-Datasheet.pdf, 2014. Accessed date: 2018-01-22.

[57] Agilient technology. Network analyzer basics. Technical report, Agilient technology, 2005.

[58] M. Tiuri, A. Sihvola, E. Nyfors, and M. Hallikaiken. The complex dielectric constant of snow at microwave frequencies. *IEEE Journal of Oceanic Engineering*, 9(5):377–382, 1984.

[59] AK Verma, Annapoorna BHUPAL, Zargham ROSTAMY, and GP Srivastava. Analysis of rectangular patch antenna with dielectric cover. *IEICE TRANSACTIONS on Electronics*, 74(5):1270–1276, 1991.

[60] Microwave Journal webpage. Cst studio suite 2018 released. http://www.microwavejournal.com/articles/29619-cst-studio-suite-2018-released, 2018. Accessed date: 2018-01-22.

[61] Thomas Weiland, Martin Timm, and Irina Munteanu. A practical guide to 3-d simulation. *IEEE Microwave Magazine*, 9(6), 2008.

[62] Andreas Wiesmann, U Wegmuller, Marc Honikel, Tazio Strozzi, and Charles L Werner. Potential and methodology of satellite based sar for hazard mapping. In *Geoscience and Remote Sensing Symposium, 2001. IGARSS'01. IEEE 2001 International*, volume 7, pages 3262–3264. IEEE, 2001.

[63] Norbert Yankielun, Walter Rosenthal, and Robert E Davis. Alpine snow depth measurements from aerial fmcw radar. *Cold Regions Science and Technology*, 40(1):123–134, 2004.

[64] Zyungo Yosida. Instruments and methods: A calorimeter for measuring the free water content of wet snow. *Journal of Glaciology*, 3(27):574–576, 1960.

[65] Shun-Shi Zhong, Gang Liu, and Ghulam Qasim. Closed form expressions for resonant frequency of rectangular patch antennas with multidielectric layers. *IEEE Transactions on Antennas and Propagation*, 42(9):1360–1363, Sep 1994.